CHARLES UNIVERSITY

Faculty of Science

Department of Biochemistry

Study programme: Biochemistry

Branch of study: Biochemistry

Bc. Roman Tuzhilkin

The novel combinations of experimental approaches: mass spectrometry (MS) and photo-induced surface labelling, electron release (PIER), or cross-linking (PIXL)

Nové metodiky kombinace hmotnostní spektrometrie (MS) se světlem aktivovaným povrchovým značením, elektronovým přenosem nebo síťováním (PIXL)

DIPLOMA THESIS

Supervisor: doc. RNDr. Miroslav Šulc, Ph.D.

Consultant: prof. RNDr. Antonín Vlček, CSc.

Prague 2020

Prohlásení

Prohlašuji, že jsem závěrečnou práci zpracoval samostatně a že jsem uvedl všechny použité informační zdroje a literaturu. Tato práce ani její podstatná část nebyla předložena k získání jiného nebo stejného akademického titulu.

V Praze dne 15. 6. 2020 .....

Acknowledgment

I would like to thank my tutor doc. RNDr. Miroslav Šulc, Ph.D. for his invaluable supervision and support both in the lab and during lengthy consultations without which this thesis would not have been completed at all. My gratitude also goes to every member of the team in our lab for their help with the experiments, insight and advice. Finally, I express my unending gratitude to my parents for being my most reliable and stringent correctors and redactors and helping me iron out even the most minor errors in the text.

I would also like to thank Grant agency of Charles University (GAUK n. 1538119) and Grant agency of Czech Republic (20-28126S) for financial support of this diploma thesis.

Roman Tuzhilkin

Abstract

Countless electron transport/transfer (ET) processes occur in living organisms every day. Therefore, their study is a crucial field of modern structural and functional proteomics. In many cases model proteins like azurin from *P. aeruginosa* are utilised in experiments. This blue copper protein is favoured due to a characteristic absorbance maximum at 630 nm in Cu(II) redox state of the central Cu atom. During its oxidation to Cu(I) state the A_{630} value decreases allowing UV-Vis detection of ET reaction progress.

We have introduced a structural photoinducible analogue of canonical amino acid Met – L-2-amino-5,5-azihexanoic acid (photo-Met) – into azurin structure to study oligomerization in solution *via* photo-induced cross-linking (PIXL). Using previously optimised protocols for recombinant expression in *E. coli* B834 we have inserted photo-Met into azurin moieties: wild type azurin and Az2W mutant where two adjacent W residues with confirmed role in electron hopping across protein-protein interface are present. The incorporation percentage of photo-Met in analysed samples was determined after SDS-PAGE and in-gel protease digestion *via* MALDI-TOF MS. PIXL was employed to study azurin-azurin interaction and oligomerization under different total concentrations of protein (in range of 15–300 μM). The samples were exposed to intense UV light and the results were evaluated *via* SDS-PAGE and UV-Vis spectrophotometry. SDS-PAGE protein band relative mobility 28−30 kDa corresponding to dimer was observed and MALDI-TOF MS and LC-MS/MS were employed after in-gel proteolysis to confirm protein moiety and determine XL identity, respectively. We have observed higher dimerization yield with increasing total azurin concentration in solution and generally increased dimer formation in Az2W mutant compared to wild type azurin under lower protein concentrations. Simultaneously, UV-Vis spectra of studied azurins before and after UV irradiation suggest that during PIXL experiment a significant decrease of A_{630} value occurs, probably implicating a change in redox state of central Cu atom. This intriguing effect was not observed in control Met-containing azurins to such degree.

Our findings support the role of two additional W residues on the interacting surface (formed by a β-sheet close to Cu centre) not only during intermolecular ET hopping but also in azurin oligomerization. They also widen our horizons and introduce a potential application of photo-Met for ET reaction initiation in proteins, a novel and promising technique which warrants further research.

Keywords: mass spectrometry, photo-induced surface labelling, electron release (PIER), cross-linking (PIXL)

Abstrakt

V živých organismech probíhá každým okamžikem nespočet dějů s účastí přenosu/transportu elektronu (ET). Proto jejich studium je důležitým cílem moderní strukturně-funkční proteomiky. Pro řadu experimentů byl a je používán modelový protein azurin z *P. aeruginosa*. Tento modrý protein obsahující centrální atom mědi má charakteristické absorpční maximum při 630 nm v redoxním stavu Cu(II). Během jeho oxidace na Cu(I) dochází k poklesu hodnoty absorbance při 630 nm (A_{630}) a tak lze UV-Vis spektra použít pro sledování průběhu jeho ET reakcí.

Naším cílem bylo vložit světlem aktivovatelný strukturní analog kanonické aminokyseliny Met – L-2-amino-5,5-azihexanovou kyselinu (foto-Met) – do sekvence azurinu a využít vzniklý proteinový produkt pro studium oligomerizace azurinu v roztoku pomocí techniky světlem iniciovaného síťování (PIXL). Použitím optimalizovaných protokolů pro rekombinantní expresi v *E. coli* B834 jsme vložili foto-Met do přirozeného azurinu a konstruktu Az2W, ve kterém jsou přítomny dva blízké Trp, u kterých byla potvrzena role při elektronovém přeskoku („hopping“) napříč protein-proteinovým rozhraním. Míra inkorporace foto-Met do sekvence proteinů byla určena pomocí MALDI-TOF MS po separaci proteinů na SDS-PAGE a štěpení proteasou v gelu. Pomocí metody PIXL byl studován vliv rostoucí celkové koncentrace proteinu (v rozsahu koncentrací 15–300 μM) na míru interakce azurin-azurin. Vzorky byly po jednominutovém ozáření intenzivním UV světlem analyzovány a vyhodnoceny pomocí UV-Vis spektroskopie a SDS-PAGE, která prokázala tvorbu proteinového proužku o relativní mobilitě 28−30 kDa. Tento nový produkt odpovídá molekulové hmotnosti dimeru azurinu a jeho MALDI-TOF MS analýza a LC-MS/MS analýzy prokázaly, že se jedná o produkt azurinu. Současně měly posloužit k určení struktury vytvořeného zesítění. Intenzita tvorby dimeru rostla spolu se vzrůstající koncentrací azurinu v roztoku a v případě Az2W byla intenzivnější ve srovnání s WT při nižších hodnotách koncentrací azurinu v roztoku. Současně, srovnání UV-Vis spekter před a po UV ozáření vzorků během PIXL experimentu vedlo k odhalení značného poklesu hodnoty A_{630}, který pravděpodobně naznačuje změnu redoxního stavu centrálního atomu Cu. Tento neobvyklý efekt nebyl pozorován v takové míře v kontrolním experimentu s azuriny obsahujícími Met v sekvenci.

Naše výsledky potvrzují roli dvou Trp na interakčním povrchu (je tvořen β-listem v blízkosti aktivního centra) nejen při intermolekulárním elektronovém přeskoku, ale i při vlastní oligomerizaci azurinu. Získané výsledky otevírají novou cestu možného metodického přístupu pro studium ET reakcí v proteinech a pro výzkumné využití foto-Met při jejich iniciaci.

Klíčová slova: hmotnostní spektrometrie, světlem aktivované povrchové značení, elektronový přenos (PIER), síťovaní (PIXL)

(V angličtině)

Contents

List of abbreviations

A_x	absorbance at x nm
ACN	acetonitrile
All-Phe	a protein mutant where all W and Y were replaced with F (for azurin means combined mutations W48F, Y72F and Y109F)
amp_{100}	ampicillin at 100 μg/mL concentration
AzWT	wild type azurin
Az2W	azurin mutant H83Q K122W T124W T126H All-Phe
BCA	bicinchoninic acid
BCP	blue copper protein
BSA	bovine serum albumin
c	concentration ($mol.dm^{-3}$, unless stated otherwise)
CBB R-250	Coomassie Brilliant Blue R-250
cDNA	complementary DNA
CryoEM	cryo-electron microscopy
Da	Dalton, a unit of mass
dH_2O	deionized water
DMEM-LM	Dulbecco's Modified Eagle Limiting Medium
dmp	4,7-dimethyl-1,10-phenantroline
DSG	disuccinimidyl glutarate
DSS	disuccinimidyl suberate
ε	molar attenuation coefficient (M^{-1} cm^{-1}, unless stated otherwise)
E^o	standard reduction potential
EDC	1-ethyl-3-(3-dimethylaminopropyl)carbodiimide
EDTA	ethylenediaminetetraacetic acid
ESI	electrospray ionization
EPR	electron paramagnetic resonance

ET	electron transfer/transport
EtMf	ethylmorpholine
FT-ICR	Fourier-transform ion cyclotron resonance MS analyser
FPLC	fast protein liquid chromatography
IAA	iodoacetamide
IPTG	isopropyl-β-D-1-thiogalaktopyranosid
λ	wavelength (nm, unless stated otherwise)
LB	lysogeny broth
MALDI	matrix assisted laser desorption/ionization
MM-M9	mineral medium M9
MS	mass spectrometry
MW	molecular weight
m/z	mass/charge
NHS	N-hydroxysuccinimide
NMR	nuclear magnetic resonance
NN	diimine ligand
OD600	optic density at 600 nm
ρ	mass concentration
PBS	phosphate buffered saline
pH	negative common logarithm of H_3O^+ ion activity
phen	1,10-phenantroline
pI	isoelectric point
PIER	photo-induced electron release
PIXL	photo-induced cross-linking
q	quadrupole MS analyser
$Re^{I}(CO)_3(NN)X$	rhenium tricarbonyl complexes with diimine ligands
RPM	revolutions per minute

SDS-PAGE	sodium dodecyl sulfate-polyacrylamide gel electrophoresis
SHE	standard hydrogen electrode
SOC	super optimal broth with catabolite repression
TFA	trifluoroacetic acid
TOF	time of flight MS analyser
tpy	2,2':6',2'-terpyridine
Tris	tris(hydroxymethyl)aminomethane
UV	ultraviolet range of electromagnetic radiation (10–400 nm)
v/v	volume concentration
w/v	mass concentration
Vis	visible range of electromagnetic radiation (400–700 nm)
XL	cross-linking

1. Introduction

Numerous (bio)chemical reactions occur in every living organism throughout the day. One of the most common types of such reactions are redox reactions. They are fundamental for every living being, from the simplest prokaryotes to the most complex mammals and embryophytes. Their particular category is a group of electron transport/transfer (ET) reactions which play a key role in energy metabolism (e.g. photosynthesis or respiratory chain) and many redox enzymatic reactions such as secondary metabolism (e.g. biotransformation of xenobiotics). It is no surprise that understanding of the underlying mechanism of those fundamental biochemical processes was always an attractive area of research.

During the 20th century multiple hypotheses were proposed to describe the mechanism of ET in proteins. According to some of them, electrons treat protein as a homogenous medium and do not follow any specific pathways through the structure. Other presumption claimed that ET in a protein is a strictly and well-defined process with a particular designated pathway through specific amino acids, co-factors and ligands [1]. Nowadays we believe that structure of a protein or protein complex has a serious impact on ET process and electrons travel through specific bonds in a molecule. The dawn of quantum physics in the middle of 20th century, especially discovery of wave-particle dualism, introduced another extremely complex parameter to the description of ET processes in biomolecules (e.g. effects like electron hopping and tunnelling). They describe some very fast electron transfers or transfers over long distances (e.g. over 80−100 Å in respiratory chain) that are not possible in the realm of classical physics [2–4]. Expanding our understanding of those complex mechanisms can definitely be considered one of the holy grails of 21st century chemistry [5].

1.1. Approaches to electron transfer research

It is obvious that study of ET reactions is complicated and requires application of wide spectrum of approaches ranging from *in silico* prediction programs [6] to time-resolved spectroscopy experiments [7]. Due to high variability of ET systems in most cases well-studied model proteins such as cytochrome c, plastocyanin or azurin are commonly used.

One possible group of approaches, which can be referred to as *static*, does not actually involve direct observation of ET reaction. Instead, suspected key amino acids in (or close to) an active site of protein of interest are altered employing site directed mutagenesis and electrochemical properties (primarily redox potential but also EPR data [8] or enzyme activity for corresponding donor-acceptor ET reaction in oxidoreductases) of resulting mutants are studied. Coupled with structural data (e.g. NMR or X-ray crystallography) of active site's primary and secondary coordination spheres, information acquired in this approach can shed light on role of specific amino acids and their interactions and properties [9] in ET processes. An example of such approach is provided in chapter 1.3.1, p. 16 where role of weak axial ligands in azurin active

site are discussed. The main drawback is that static experiments do not provide us with in-depth detailed information about an ET process but only give some clues towards its mechanism. Additionally, necessity to prepare a wide variety of mutants severely limits throughput of such experiments.

As a result, more direct or *dynamic* time-resolved methods are often employed in ET research. One of the major challenges for those techniques is finding a reliable way of initiating the ET process and a measurement technique which will be suitable for different timescales since ET rates span a large range from picosecond to seconds [10].

Slower ET reactions (> ms) can be studied via transient-state spectroscopy such as stopped flow techniques but they are not applicable for fast reactions due to sample-mixing/diffusion limitations [11]. Electrons can also be rapidly injected into redox proteins by laser photoexcitation methods (for example of naturally occurring or artificially introduced W) which can be employed in both solution and in crystals [12,13]. Radiolysis is another approach to study ET within proteins which uses a rapid pulse of electrons to generate radicals to initiate subsequent intramolecular ET [14]. From large part, our understanding of ET processes comes from methods which employ exogenous photoexcitable electron donors (for example Ru and Re complexes discussed in chapter 1.6.1, p. 26 but also a wide variety of others [15–17]) which act as an initial precursor compound for a subsequent intramolecular ET reaction in spectroscopic flash-quench experiments.

It is worth noting, that this brief overview does not even begin to scratch the surface of wide variety of approaches which can be employed for ET studies, each offering unique and valuable advantages but also drawbacks and challenges. Many of those methods are still commonly employed in ET experiments and this only serves to underline the complexity of the problem they are designed to solve. One might claim that even despite this already existing variety other novel approaches to ET research could still be invaluable help in bringing us closer to complete understanding of this fascinating biochemical phenomena and are thus worth pursuing.

1.2. Copper ion in proteins - cupredoxines

Copper ion is one of the two most common metal ions that participate in ET processes in proteins. It can be found in many proteins with wide spectrum of functions in the organism. Cu-complexes can be divided into several structural types: types 1–3, CuA, CuB and CuZ [18]. Type 1, also known as “blue copper”, contains a single Cu ion, usually participates in single electron transfers and can be found in some oxidoreductases and cupredoxines.

Cupredoxines (also known as Blue Copper Proteins or BCPs) are a family of small proteins (usually 90–160 amino acids) which can be found in respiratory chain of several species where they act as single electron transporters with E^{o} ranging from 100 mV to 800 mV (vs. SHE, standard hydrogen electrode) [9]. The Cu atom in the active site of cupredoxines is held in place

via three equatorial ligands (two imidazole ring nitrogen atoms of two His and one sulfur atom of Cys). In some cases, a weaker axial ligand, sulfur atom of Met, is present. Since the axial ligand is located farther away from the Cu ion (2,8–3,1 Å) the bond between them is weaker. The examples of this active site can be found in plastocyanin (see Figure 1, A), rusticyanin and some forms of nitrite reductase and ascorbate oxidase [19]. The active site of azurin (Figure 1, B) is slightly different from canonical type 1 active site. Unlike other BCPs Cu ion in azurins has two axial ligands, a previously mentioned sulfur of Met (3,2 Å away from Cu) and an oxygen atom of carbonyl group of Gly (2,8 Å away from Cu). As we will see later (see chapter 1.3.1, p. 16), despite their weaker bond axial ligands can have a significant influence on protein active site.

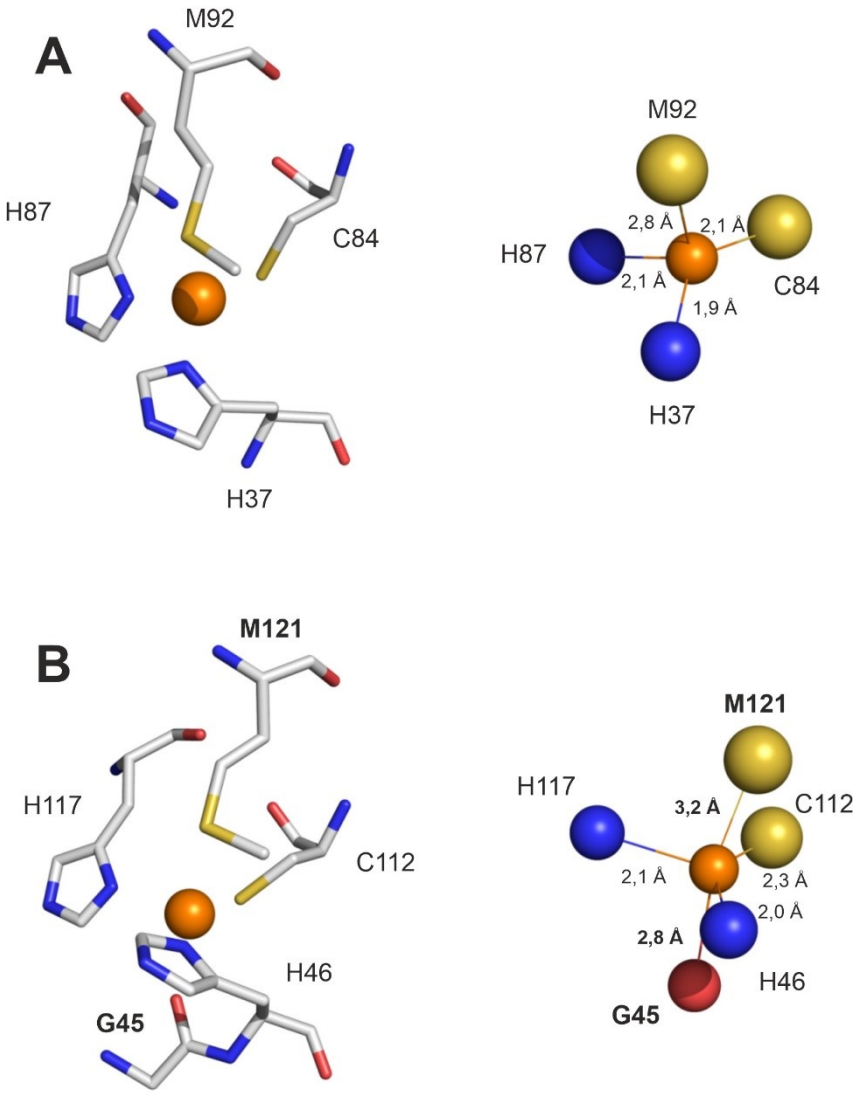

Figure 1 Representative type 1 Cu active sites in BCPs. **A** – Plastocyanin from *Populus nigra* (PDB code 1PLC), the most common arrangement with two equatorial His, an equatorial Cys and axial Met in primary coordination sphere of Cu. **B** – Azurin from *P. aeruginosa* (4AZU), where an additional axial ligand, an oxygen of a carbonyl group of Gly is present. Geometry of copper (orange) and its ligands atoms (nitrogen in blue, sulfur in yellow, oxygen in red) is shown to the right.

1.3. Azurin, the basic overview

Azurins are small (120–130 amino acids) electron transport proteins, which can be found in several bacterial species and contribute to electron transfer during anaerobic respiration and denitrification pathways.

Azurin is commonly used as a model protein for studying electron transfer in biological systems. Since 1970s modified azurins with donor-acceptor complexes were used to test and verify electron transport hypotheses [20–22]. Azurin is still commonly used to study the role of specific amino acids in electron transfer proteins. Based on this model protein the forces providing protein stability and active site structure formation [23] as well as relative stability of Cu ions redox states [24] were determined (e.g. Cu(II) redox state stabilization by the weak axial coordination of carbonyl group oxygen [25]). Azurin has a well conserved structure and its properties can be altered by introducing an artificial active site or an active site of another cupredoxine into the structure of wild type azurin [26]. Role of a metal ion in formation and stabilization of metalloprotein 3D structure was determined using an azurin model [23,27]. To give an example, the presence of metal ion significantly stabilizes the protein (melting temperature: 62 °C for apo-azurin, 80 °C for Cu-azurin and 90 °C for Zn-azurin). The characteristics of the metal ion itself also play a significant role and the denaturation enthalpy of Cu and Zn substituted azurin is higher than in case of Ni, Ag or Mn carrying forms [28]. It is also worth noting that anticancer, antiparasitic and antivirotic activity was observed in peptides derived from azurin primary structure [29].

The structure of azurin is highly conserved through a number of species. As all BCPs, azurins have the classical β-barrel Greek key three-dimensional structure. Compared to plastocyanin, wild type azurin (AzWT) is slightly larger and harbours an additional α-helix as shown on Figure 2, A, p. 15 [30,31]. The C-terminal β-sheet in azurin structure deserves particular attention since it harbours amino acids participating in both ET processes and protein-protein interaction in azurin dimer [32]. The second structure on Figure 2, B, p. 15 is azurin mutant H83Q K122W T124W T126H All-Phe (meaning a combined mutation W48F Y72F Y108F where all W and Y naturally occurring in wild type azurin were replaced with F), which will be further referred to as Az2W (due to the double-W bridge/"pier" in positions 122 and 124), with mutations located on this C-terminal β-sheet highlighted. Despite the mutations, overall structure of the protein remains largely unchanged.

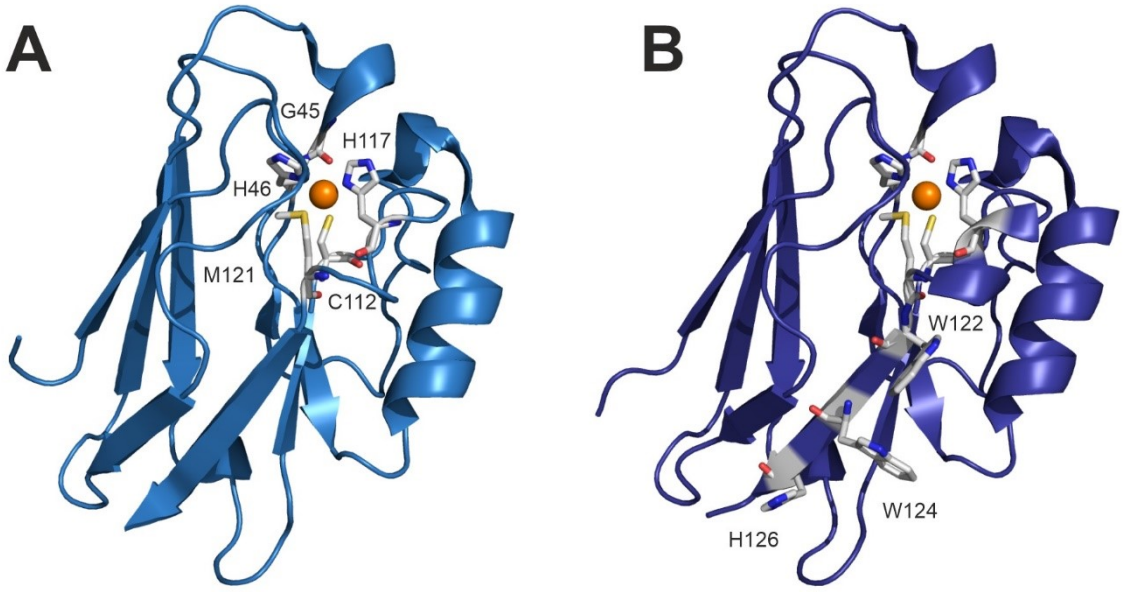

Figure 2 **A** – Structure of wild type *P. aeruginosa* azurin (4AZU) with highlighted Cu atom (orange) coordinated *via* side chains of amino acids (His, His, Cys, Met) and carbonyl oxygen of Gly. **B** – Structure of H83Q K122W T124W T126H All-Phe azurin mutant (6MJS) with altered amino acids located on C-terminal β-sheet.

The metal binding site has a well-defined and rigid geometry which leads to unique coordination of Cu in azurin and other BCPs. *Pseudomonas aeruginosa* azurin active site is representative of common azurin active site mentioned earlier. Redox active Cu ion is coordinated in trigonal bipyramid geometry *via* three equatorial ligands: two imidazoles of H46 and H117 and thiol group of C112 and two axial ligands: sulfur atom of M121 and carbonyl of G45.

Azurin exhibits spectral properties similar of other cupredoxines – a characteristic intense absorbance peak (attributed to $S(Cys)_{\pi} \rightarrow Cu(II)d_{x^2-y^2}$ ligand-to-metal charge transfer transition [33]) at 630 nm is present in their visible spectra (ε ~5700 M^{-1} cm^{-1} [34]). The pI of azurin varies noticeably depending on the presence/absence of the metal ligand, its characteristics and redox state. As such apo-azurin has a pI of 5,4 and after binding of Cu(II) the value increases slightly to 5,6. In reduced form Cu(I)-azurin exhibits much lower pI at 4,6. Isoelectric point of Zn(II)-carrying azurin is 5,4 [35]. As all other cupredoxines, azurin is capable of participating in ET and its redox potential (for wild type *P. aeruginosa* azurin, vs. SHE) is ~310 mV at pH 7 [33].

In *in vitro* experiments other metallic ions such as Ni can bind into the active site (with subsequent shift of E^{o} value to –800 mV [24]). Azurins with Zn, Co, Fe and even Ag in the active site have been previously reported [36–38]. The crystal structures in case of binding of a different metallic cofactor or its absence (apo-protein) are nearly identical (Figure 3, p. 16). A certain exception from this is Zn-carrying azurin where the active site is distorted compared to Cu-azurin. In Zn-azurin the axial Met is no longer coordinated to the central metal ion despite their geometry remaining largely unchanged (3,3 Å distance between Zn and M121 in Zn-azurin crystal structure 1E67). As a result, the bond between Zn and the other axial ligand, oxygen

atom of carbonyl group of Gly, becomes stronger (0,23 nm vs. 0,29 nm in Cu-azurin) [36]. More than that, since oxidation states other than Zn(II) are not accessible for zinc in proteins, Zn-azurin is not redox active and lacks characteristic spectroscopic properties due to spectroscopically "silent" d10 system of zinc atom [24].

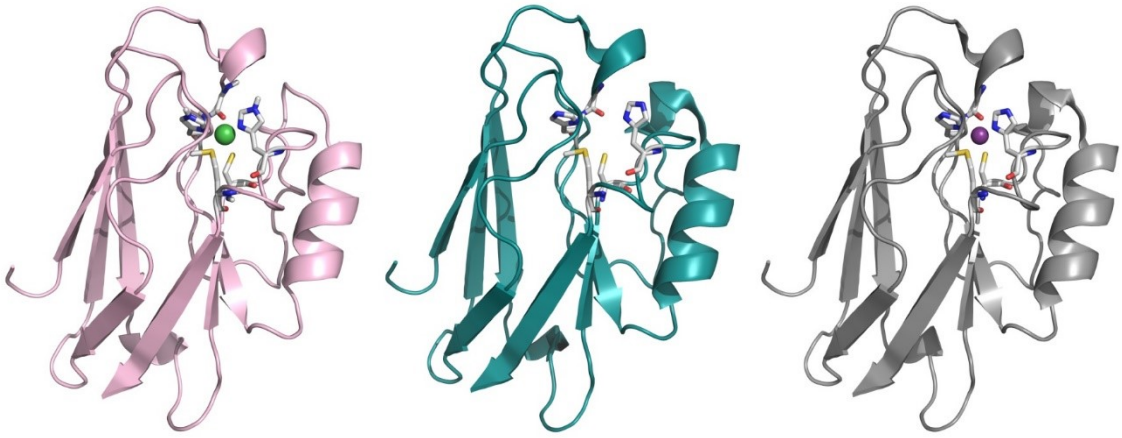

Figure 3 Azurin structures with unorthodox metal cofactors. **Pink** – Ni-azurin (1NZR, Ni atom in green), **cyan** – apo-azurin (1E65), **grey** – redox inactive Zn-azurin (1E67, Zn in violet). Overall protein fold and specific geometry of the active site show only minimal variation between the structures even when compared to Cu-azurin (Figure 2, p. 15)

1.3.1. When weak ligands matter, fine tuning of azurin redox potential

It has been already mentioned earlier, that despite relatively weak bond between axial ligands and metal ion in BCPs and type 1 Cu centres in general, alterations to those ligands can lead to major changes in protein properties.

Experiments with azurin have showed that the presence of a hydrophobic residue (for example Leu) instead of the axial Met leads to increase in E^o by 40–160 mV while a more polar amino acid like Gln at the same position decreased the reduction potential by 100–260 mV [9,39]. In some studies the use of unnatural amino acids derived from Met (thioether group of Met replaced with other functional groups, most notably ether and alkyl carbon) in place of Met121 has allowed azurin derivatives to cover the span of redox potentials from 200 to 500 mV [40].

The role of the other axial ligand, a carbonyl oxygen of Gly has already been briefly mentioned earlier and can be illustrated by comparing redox potentials of azurin (E^o ~310 mV) and rusticyanin (E^o ~670 mV at pH < 3 [33]) in which this axial ligand is not present. Significantly lower E^o value in azurin (and most other BCPs when compared to rusticyanin) can be explained by increased electron density around Cu atom caused by the ionic interaction with the carbonyl oxygen of Gly which stabilizes the Cu(II) state [25].

Outside of aforementioned modifications of axial ligands other alterations in key amino acids in *P. aeruginosa* azurin sequence (notably to Met44, Asn47, Trp48 and Phe114) can have a significant effect on its E^o value. To give an example, Asn47Ser mutation also resulted in an increase in the reduction potential since its effect leads to strengthening of the H-bonds to a Cys

ligand and rigidification of the active site. On the other hand, replacement of Phe114 with Pro resulted in disruption of active site and removal of H-bond to Cys which has led to decrease in E^o [9].

Azurin E^o value is also dependent on pH (see Table 1) and as is the case for majority of other redox proteins exhibits moderate decrease with increasing pH.

Due to the fact that, as a general rule, the effects of different modifications to azurin active site are additive it was possible to design azurin derivatives with E^o ranging from –1 V to 1 V [24,25]. These experiments highlight azurin's surprising ability to cover a wide range of naturally occurring redox potentials. Table 1 shows some of the modifications to azurin sequence and their effect on E^o under different pH.

Table 1 An overview of single amino acid mutations in primary/secondary coordination sphere of *P. aeruginosa* azurin active site and their effect on protein redox potential at different pH (in mV vs. SHE). Highlighted in bold are modifications used to illustrate additive effect of individual mutations in double/triple mutants (last four rows). Based on [9,25].

Protein	pH				
	4	5	6	7	8
Wild type		346	333	310	293
His35Lys		344	337	317	296
Met44Phe	434	428	412	384	373
Gly45Ala		333	314	300	292
Asn47Asp				333	
Asn47Ser				396	
Trp48Leu		352	345	323	306
Ser89Gly	354	339	312	294	288
Phe114Ala		377	372	358	343
Phe114Pro				181	
Phe114Asn				398	
Met121Leu			433	412	392
Met121Ala				373	
Met121Asp			333	319	287
Met121Gln				195	
Met121Lys				318	
Met121Gln + Phe114Pro				92	
Met121Gln + Asn47Ser				225	
Met121Leu + Asn47Ser				496	
Met121Leu + Phe114Asn + Asn47Ser				640	

1.3.2. Oligomerization of azurin

In some experiments oligomerization of azurin and its mutants was observed [41]. Weak transient oligomers are formed and in a concentrated solution a varied size distribution can be observed with some oligomers reaching up to 11-mers. In less concentrated solution (70 μM) only high amounts of dimer can be found. Azurin is mostly present in the form of monomer in solutions of low concentration (< 70 μM) although small amount of dimer is formed and can be observed using cross-linking techniques even at very low concentrations [42,43]. It is also worth noting that asymmetric units of some X-ray structures of azurin (e.g. structure 4AZU [44]) are commonly formed by two or four molecules of the protein.

Oligomerization can affect ET processes occurring in the protein and has to be taken into consideration when azurin is used as ET model. Last year Takematsu et al. published an ET study on azurin mutants labelled with Re complexes which revealed abnormally high ET rate through the protein in Az2W mutant. Their proposed explanation for this observation (see Figure 4) is formation of azurin dimer where extremely fast intermolecular ET can occur over much shorter distance than in case of intramolecular ET [32].

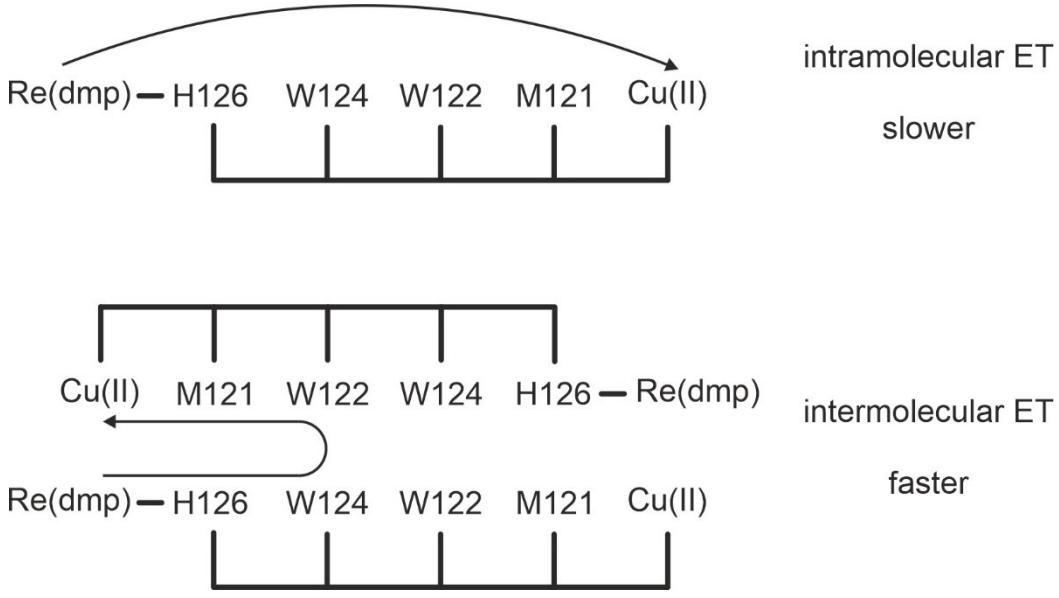

Figure 4 Proposed mechanism of ET transport processes occurring in H83Q K122W T124W T126H azurin mutant. **Top** – a much slower intramolecular transfer observed in most mutants. **Bottom** – explanation for the fast ET occurring due to dimerization of the protein. Arrows are used to represent the general flow of electrons and do not depict specific path an electron takes.

1.4. Cross-linking

In recent decades complete proteomes of many organisms have been solved. But in many cases, little is known about functions of many proteins and even less is known about their mechanism of action. There are multiple approaches to solving function of proteins and one of them is its relation to structure. Information about tertiary and quaternary structure of a protein or protein complex can provide us with invaluable insight into its potential partners, ligands or coenzymes

and the way they interact with each other. High-resolution techniques like X-ray crystallography or NMR provide very detailed structural characterization but are often limited in their application. They are not suitable for *in vivo* experiments and in case of X-ray even experiments in solution and require high amounts of purified and suitably modified protein. In the last couple of years cryo-electron microscopy (CryoEM) has emerged as a new cutting-edge high-resolution technique which solves several of these limitations [45]. It allows determination of macromolecules at near-atomic resolution, without the need for crystals [46]. Despite that, its application is still limited due to extreme financial costs of required precise instrumentation. But even if we were to overlook those financial burdens, CryoEM carries similar major disadvantage like X-ray crystallography – both of those approaches are only suitable for study of static molecules. All of the information about dynamic events occurring in the sample is lost due to sample preparation protocol (crystallization or freezing, respectively) required for those techniques. The third technique mentioned here – NMR – allows to study biomolecules in solution so dynamic events can be observed but several factors limit its application. Very high non-physiological concentration of very pure protein is required for the experiment which is also time consuming and is not suitable for unstable proteins or faster dynamics (low dynamic resolution). The cost of an NMR experiment is high due to necessity to label proteins with NMR active ^{13}C or ^{15}N and large molecules with high molecular weight (> 60 kDa) are still problematic for this technique.

Because of that many other low-resolution approaches were developed. Despite of the fact that they cannot provide full structural information, they are still able to give us leads to uncover function of studied protein and provide us with valuable information on dynamic processes occurring in the sample. Cross-linking (commonly abbreviated XL) is one of those techniques which is experiencing a renaissance in the last two decades due to recent development in the field of mass spectrometry (MS). The goal of the approach is to build up a set of structurally defined interactions by covalently connecting pairs of functional groups within a protein or a protein complex. The location of the formed cross-links imposes a distance constraint on the location of the respective side chains and allows drawing conclusions on the distance geometries of a protein or a protein complex structure [47–49].

Despite providing less structural information when compared to high-resolution techniques, at the same time XL offers several valuable advantages. Cross-linking experiments are always carried out in solution at physiological protein concentration, so no information about dynamics is lost. Additionally, certain XL protocols allow studies under both *in vitro* and *in vivo* conditions (discussed later in the chapter). Finally, valuable amount of protein required for an XL experiment compared to X-ray crystallography or NMR and no modifications like crystallization or ^{13}C labelling are required which simplifies sample preparation and allows higher experimental throughput.

1.4.1. Cross-linking strategies

The protocol of an XL experiment is straightforward. Cross-linking reaction is performed and formed products are then analysed using common MS techniques. Two possible protocols are commonly referred to as bottom-up and top-down. In bottom-up approach the cross-linked products are separated from monomers and then each of them is enzymatically cleaved, and the resulting mixture of peptides from each individual protein form/arrangement is analysed using MS. Intermediate steps often include purification of cross-linked product using SDS-PAGE followed by in-gel digestion or chromatography techniques (mainly size exclusion chromatography) coupled with in-solution digestion. Top-down is a more direct approach where intact cross-linked products are analysed without enzymatic digestion using electrospray ionization Fourier-transform ion-cyclotron resonance (ESI-FT-ICR) mass spectrometry (particularly, intact proteins MS separation followed by MS/MS fragmentation with FT-ICR detection) [50]. Generally speaking, top-down approach is more straightforward but more demanding on MS equipment.

1.4.2. Cross-linking reaction

The major aim of XL reaction is formation of a covalent bond between two spatially proximate residues within a single or between two polypeptide chains. But quite often the reaction only occurs on one side of bifunctional cross-linker and alternatives products (which are sometimes referred to as type 0, 1 and 2, see Figure 5) are observed. Type 3 designation can be used for a product which combines all three previous types (not shown).

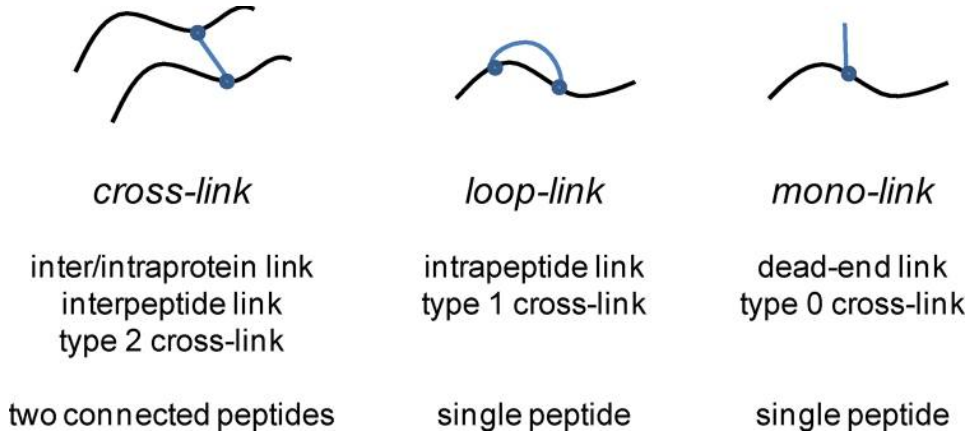

Figure 5 Nomenclature of common products of chemical XL reactions. From [51].

1.4.3. Cross-linking reagents

The most commonly utilised type of XL reagents are homobifunctional chemicals, where two reactive groups are connected by a linker region or spacer, typically an alkyl chain, of defined length. The functional groups are usually classified based on their reactivity.

Amine-reactive cross-linkers most commonly target ε-amino group of lysine and protein *N-termini*. For this purpose, N-hydroxysuccinimide (NHS) esters are almost exclusively used. NHS esters react with nucleophiles to release the NHS group and to create stable amide and imide bonds with primary or secondary amines. Their advantages include high reaction rate and specificity [52], although relatively stable products with hydroxyl groups of serine and threonine have also been reported. On the other hand, NHS esters undergo hydrolysis under typical physiological pH, which limits reaction time [53]. They also dissolve poorly in aqueous buffers and require prior dissolution in small volumes of organic solvents. Alternatively, sulfo-NHS esters – the water-soluble analogues – can be used. Although in practice most commonly, DSS (disuccinimidyl suberate) and DSG (disuccinimidyl glutarate) are employed for protein 3D structures studies. Both are homobifunctional NHS ester cross-linkers with 11,4 Å and 7,7 Å spacer arm, respectively.

Other amine-reactive groups include imido esters and carbodiimides. The former exhibit very high specificity towards lysine amino-group but their reaction has pH optimum of 8–9 [54]. The later are utilised for covalently linking an amino group with carboxylic or phosphate group [55] in close spatial proximity (< 3 Å) to create a zero-length cross-link. The most popular of carbodiimides is water-soluble EDC (1-ethyl-3-(3-dimethylaminopropyl)carbodiimide) commonly applied in combination with a sulfo-NHS ester to increase the yield of cross-linking reaction [56].

When using *sulfhydryl-reactive cross-linkers* two major obstacles when targeting SH groups of cysteine, namely low abundance of cysteine in proteins and their possible involvement in disulfide bonds, should be taken into account. Reduction of disulfide bonds to make sulfhydryl groups accessible carries a risk of disrupting protein native state/structure or even denaturation. Maleimides are an example of SH targeting cross-linking groups.

Other approaches to chemical XL include *arginine-specific cross-linking* and *acidic cross-linking*. Their use is though limited because the reactions cannot be performed under appropriate ("native") conditions or because reaction products are instable or inhomogeneous.

Other types of XL reagents include heterobifunctional cross-linkers which contain two different reactive groups (e.g. an amine and a sulfhydryl group) and can be utilised for some speciality experiments. Heterobifunctional cross-linker with one photoreactive group are also utilised due to stability of the photoreactive group before high-intensity light exposition.

The wide variety of most popular cross-linkers, their chemistry and pH optima are summarized in Table 2, p. 22.

Table 2 An overview of the most commonly utilised cross-linking reagents and their pH optima.

Cross-linker	Reaction	pH optimum
NHS esters (*amine reactive*)	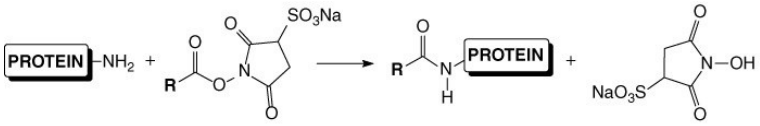	7–7,5
Imido esters (*amine reactive*)	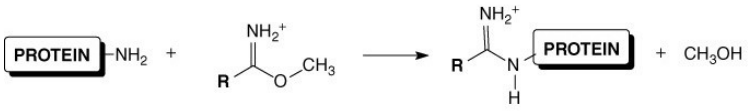	8–9
EDC (a carbodiimide) with sulfo-NHS (*amine/carboxylic acid reactive*)	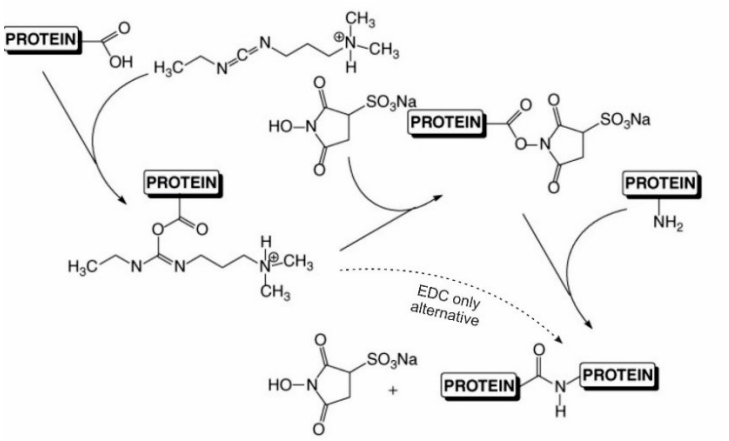	4,5–7,5 or 4,5−6,0 (EDC only)
Maleimides (*sulfhydryl reactive*)	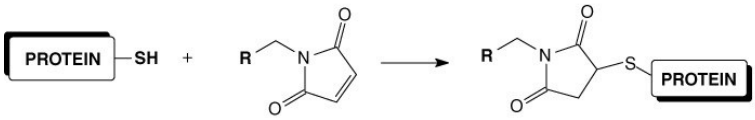	6,5–7,5
Aryl azides (*photoreactive*)	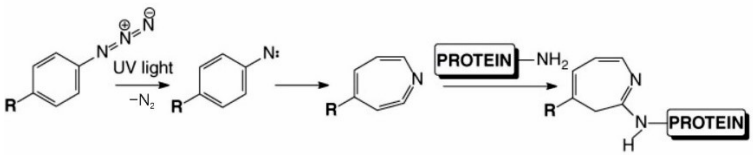	0–14

In recent years approaches that allow chemical cross-linking in living cells have been developed. Ranging from treatment of cells with formaldehyde [57] to incorporation of a unique chemical into a protein of interest, using the cell's own biosynthetic machinery [58]. In some cases, non-chemical ways of initiating cross-linking reaction can be beneficial in *in vivo* systems. For those purposes photoreactive functional groups such as aryl azides or diazirines are utilised leading to a group of approaches known as photoreactive cross-linking.

The advantages of photoreactive approaches are not only limited to their application in *in vivo* experiments. Unlike chemical cross-linkers, activity of photoreactive groups is not dependent

on a chemical reaction and thus its reactivity is less demanding on buffer composition, pH and other reaction conditions. At the same time cross-linked products of those reactions are highly stable and exhibit long lifetimes. Thanks to their high reactivity photoactivated intermediates can react non-specifically with most double bonds and active hydrogen bonds at C–H and N–H sites [59]. This allows photoreactive cross-linkers to capture interactions which might elude some chemical cross-linkers due to lack of solvent accessible reactive groups close to the interaction surface.

1.5. Photo-induced cross-linking (PIXL)

In 2005 Suchanek et al. synthesised structural analogues of canonical Met and Leu which gave them the name photo-Met and photo-Leu [60]. Those amino acids contain diazirine group that can be photoactivated with UV light (350–370 nm) yielding highly reactive carben with short lifetime in range of nanoseconds. Carben radical is unstable and rapidly reacts with its closest surroundings (under 5 Å) to create a new covalent bond (a zero-length cross-link) [61]. Alternatively, termination yielding a double bond is possible [62] (see Figure 6)

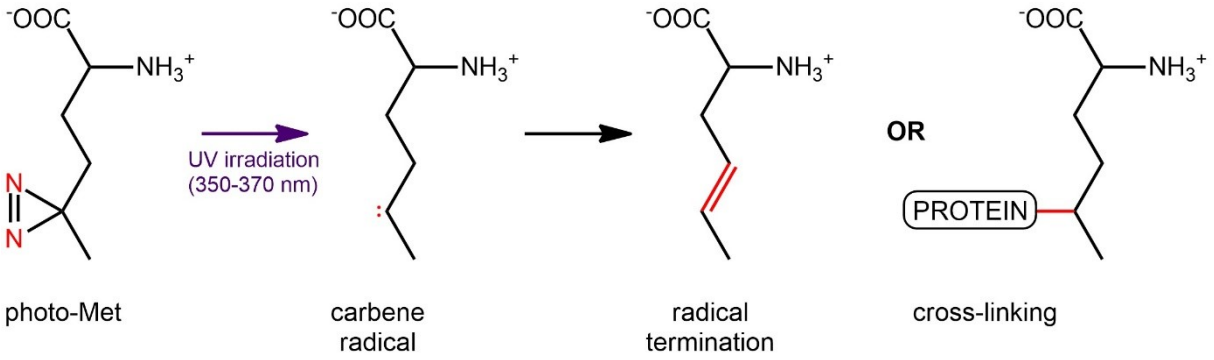

Figure 6 Structure and reaction mechanism of photo-Met. After photoactivation with UV light photo-Met yields a highly reactive carben intermediate which immediately attacks a C–H or N–H bond in its close proximity forming a cross-link or undergoes termination which yields a product with a double bond.

Significant structural similarity of photo-Met and photo-Leu to Met and Leu can be observed on Figure 7, p. 24. Because of that, they can be utilised for photo-induced cross-linking (PIXL) leading to several major benefits compared to other cross-linking techniques. Photo-Met (and photo-Leu) can react with their respective native aminoacyl-tRNA-synthetases and then be incorporated into the sequence of a synthesised protein. For PIXL experiments use of photo-Met is generally preferred due to its higher incorporation ratios (attributed to absent proof-reading activity of methionyl-tRNA synthetase which is present in Leu-tRNA synthetase [63,64]) and lower abundance of particular amino acid in proteins (1,7% for Met vs. 7,4% for Leu [65]) which simplifies distant constraints data interpretation. In most cases only minimal influence of photo-Met incorporation on functions of the expressed protein was observed. It was previously postulated in literature, that photo-analogues are not toxic for the cell and do not have major hindering effects on proteosynthesis [60].

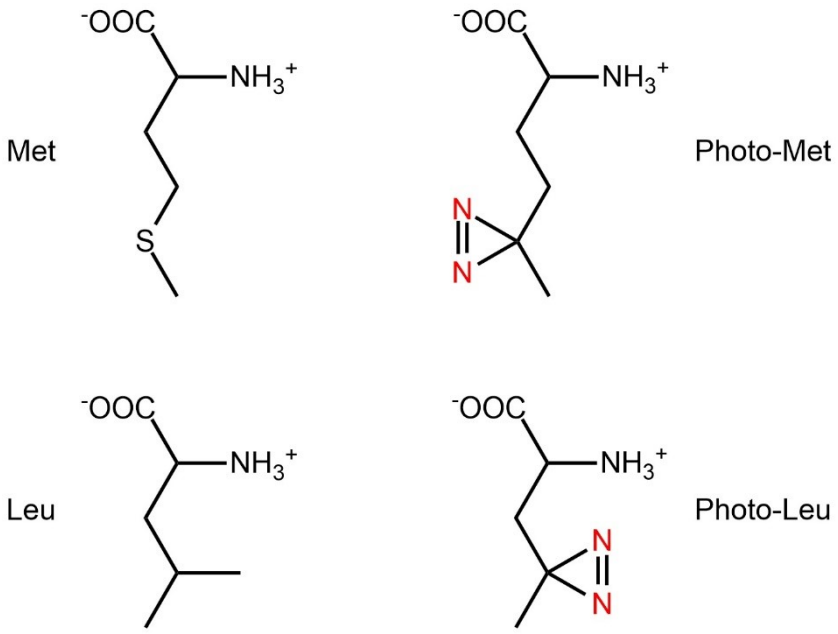

Figure 7 Structures of canonical Met and Leu (**left**) and their photoreactive analogues photo-Met and photo-Leu (**right**)

Due to that, it may seem like no special techniques are required for incorporation of photo-Met into protein sequence. Unfortunately, employing regular production *E. coli* strain only yields low degree of incorporation dependent on expression time and used photo-Met concentrations [66]. The main reason for this low yield is approx. three orders higher dissociation constant for structural analogue compared to its canonical amino acid and respective aminoacyl-tRNA-synthetase [67]. Therefore, strains of *E. coli* auxotrophic for Met, inhibitors of secondary pathways of Met synthesis, mineral mediums (e.g. M9 medium) which help decrease Met and Met-tRNA concentrations inside the cell, systems with strictly defined start of expression of protein of interest only in the presence of structural photo analogue and other techniques (the most obvious solution of increasing photo-Met concentration is limited in practice by high cost of photo-Met) have to be employed to increase photo-Met incorporation to 50–90% dependent on expressed protein and applied conditions [68].

Although aforementioned difficulties look tricky, after successful photo-Met incorporation into protein sequence the advantages of PIXL can enter the stage of experiment. The PIXL reaction of photo-Met is defined in space and time and the yield is usually high since only one bond has to be formed and due to high reactivity, low selectivity and short lifetime of carben intermediate. Additionally, the reaction is not dependent on pH or buffer composition and is not limited by requirement for a presence of specific solvent accessible reactive group on the protein surface. Formation of a covalent bond allows analysis of cross-linked products with common mass spectrometry (MS) techniques. PIXL allows zero-length cross-linking and very short-lived transient interactions can be observed even in living cells [60] or membrane environment [69].

General protocol of a PIXL experiment is summarized in the following flowchart on Figure 8.

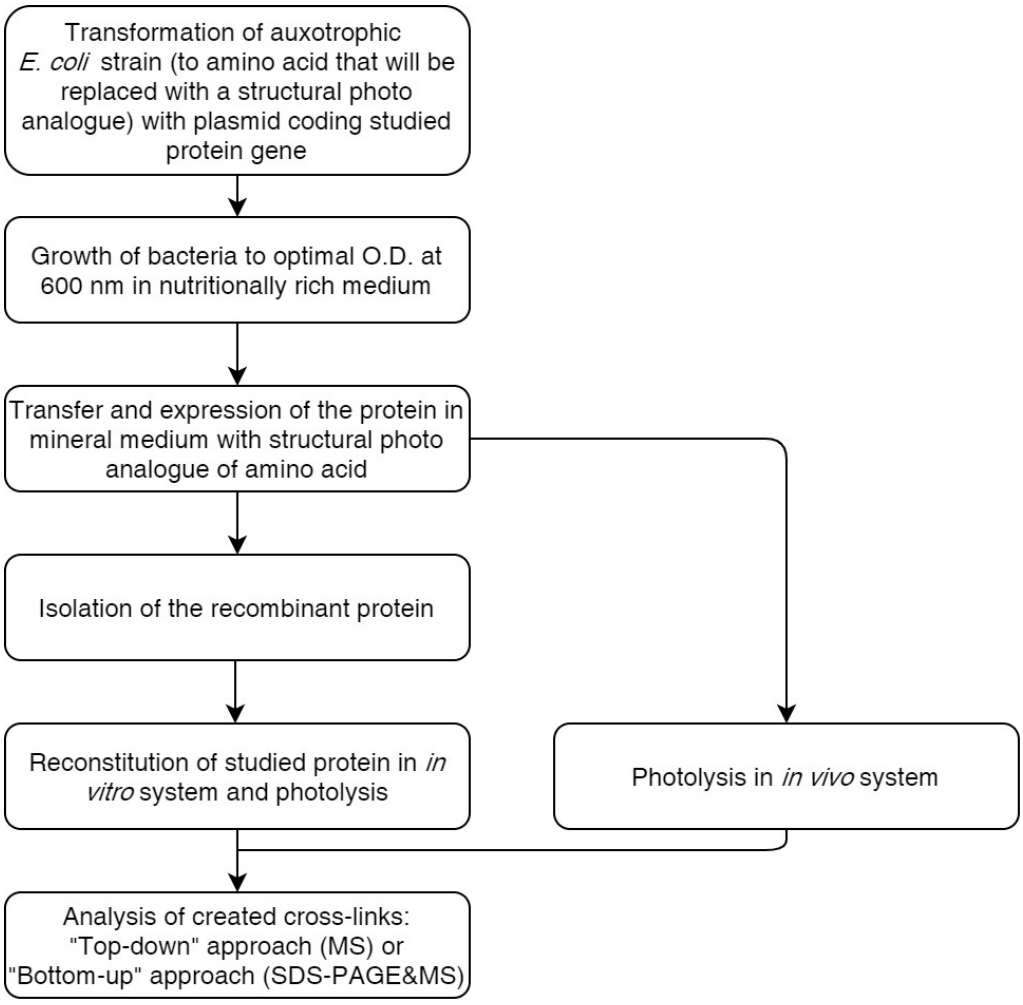

Figure 8 General flowchart of a PIXL experiment.

1.6. Photo-Met beyond cross-linking, the introduction of photo-induced electron release

Potential applications of photo-Met's properties are not necessarily limited to cross-linking experiments. Under certain circumstances a competing alternative reaction can occur. Instead of participating in formation of a new bond a carben intermediate could be a potential source of an electron which can then be released, and initiate electron transfer via a "pier" of protein structure to its redox active site (e.g. Cu(II) in azurin structure). This potential reaction pathway widens our horizons and introduces a previously unknown approach to ET initiation – photo-induced electron release (or PIER, see Figure 9, p. 26).

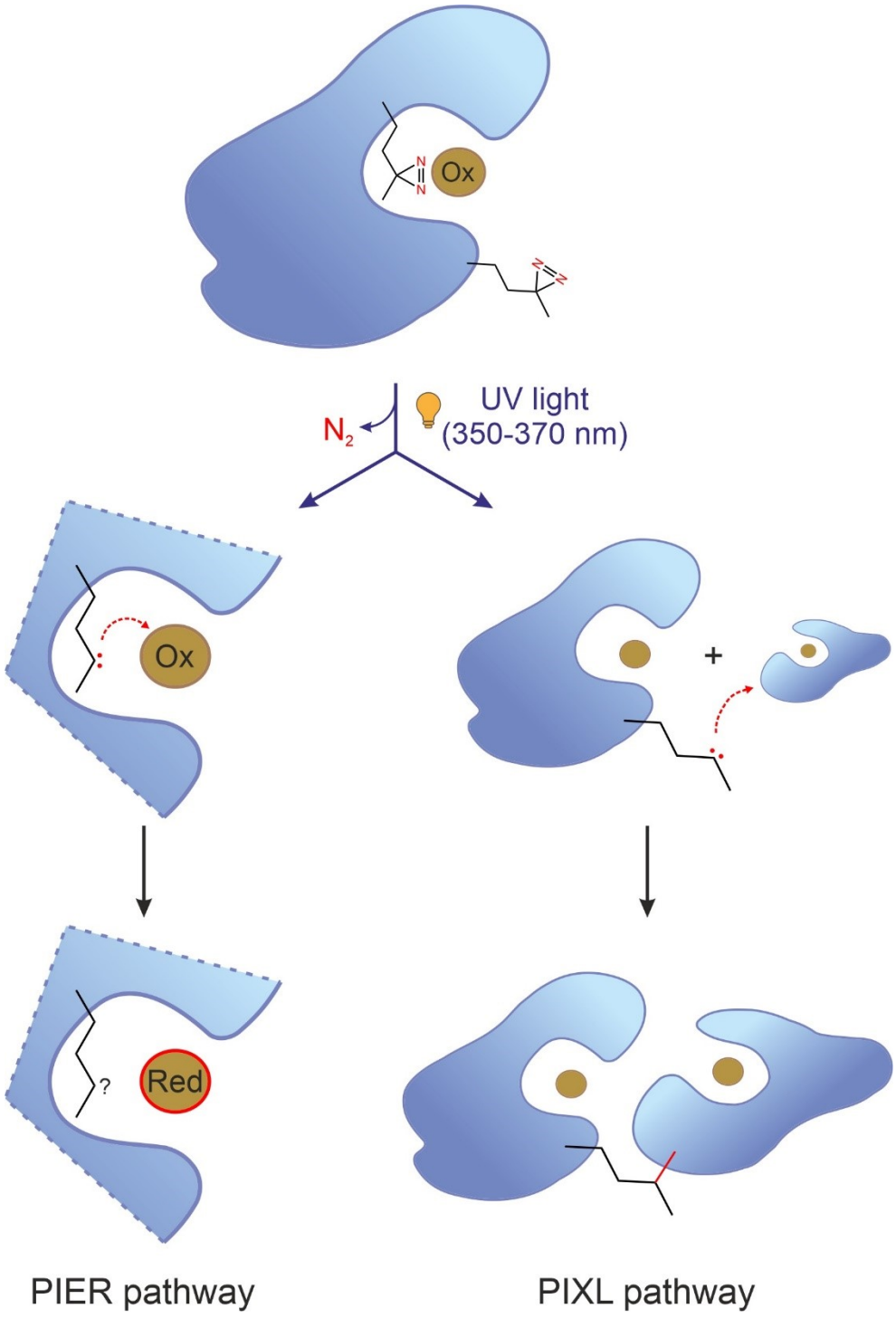

Figure 9 Mechanism of PIXL reaction next to proposed PIER pathway for photo-Met. The amino acid "pier" is omitted on the figure and electron is shown to transfer directly from carben intermediate to protein active site in PIER mechanism for the sake of image clarity.

1.6.1. Re^{I} complex labelling, a powerful and versatile (yet bulky) technique

Before further discussing PIER itself, it will be appropriate to first introduce a different already well-established ET initiation technique which we can use as our reference.

Coordination compounds like rhenium (and ruthenium) tricarbonyl complexes with diimine ligands (commonly denoted as $Re^{I}(CO)_3(NN)X$ where NN is a diimine ligand (e.g. 1,10-phenantroline (phen) or 4,7-dimethyl-1,10-phenantroline (dmp)), see Figure 10) are commonly utilised in modern chemistry across its multiple disciplines and often find a variety of applications in molecular devices. Their use is ranging from photosensitization and luminescent sensors to photocatalysts and light emitting devices [70].

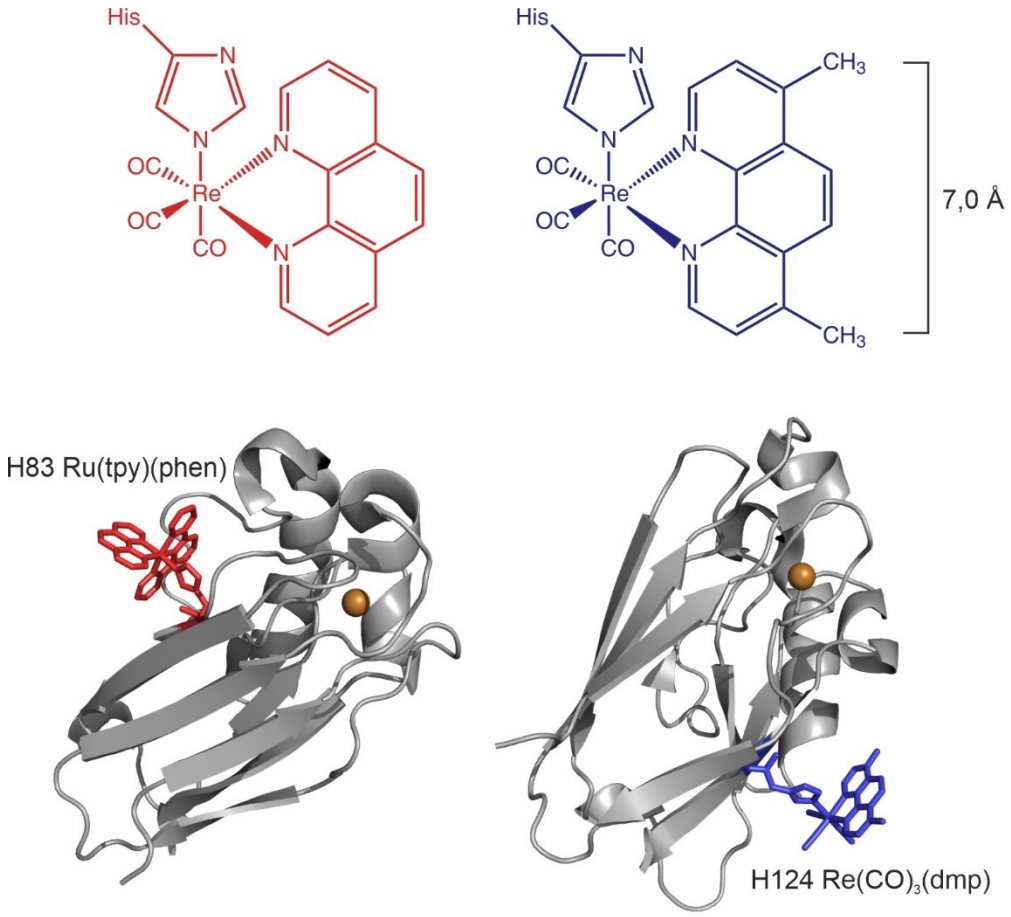

Figure 10 **Top –** Rhenium tricarbonyl complexes with diimine ligands ($Re^{I}(CO)_3(NN)X$) phen (**red, on the left**) and dmp (**blue, on the right**). In this picture the sixth ligand X is represented by an imidazole N-atom of His side chain, the residue where the complex is anchored to a protein. **Bottom –** illustrative structures of azurins labelled with Re^{I}-complexes. **To the left** is azurin with Ru(tpy)(phen) complex anchored to H83 (1JZF), **to the right** azurin mutant H83Q K122T T124H labelled with H124 $Re(CO)_3(dmp)$ is shown (2I7O). Abbreviation tpy stands for 2,2':6',2'-terpyridine.

Re^{I} complexes can also be attached to proteins *via* coordination of imidazole N-atom of a His residue on protein surface (due to bulkiness of the complex and to facilitate its regeneration at expense of solvent) and form a reactive intermediate which initiates an ET process across a protein after photoactivation (400 or 355 nm, high intensity laser). It was already mentioned previously (chapter 1.1, p. 11) that much of our understanding of biological ET is based on experiments where an exogenous photoexcitable electron donor is introduced into protein structure and utilised to initiate the reaction. To expand on this statement, it is actually structurally characterized Re^{I}- and Ru^{II}-diimine derivatives of *P. aeruginosa* azurin [71] which

form the foundation of our knowledge. Some of those derivatives have already been shown in Figure 10.

Multiple groups have applied Re^{I} complexes to study the fundamentals of ET reactions in small electron carriers like azurin [42,72,73] but also ET processes occurring in oxidoreductases like ribonucleotide reductase [74] or nitric oxide synthase [75]. The protocol for Re^{I} complex labelling is well-proven and has been applied to different proteins, the photoactivation reaction yield is usually high but one of the most crucial advantages of Re^{I}-diimine complexes is their ability to be regenerated and reused for several experiments. After donating an electron to protein molecule an expended Re^{I} label can recover an electron from water (releasing a hydroxyl radical) and return to its active state. The major disadvantages of this technique are mostly related to general bulk of $Re^{I}(CO)_3(NN)X$ which can affect native structure of studied proteins, prevent certain protein-protein interactions or generally be incapable of reaching close enough to an active site buried deep inside the structure. Another limitation arises from generally poor yield of protein Re^{I}-labelling and time-consuming protocol (incubations in range of weeks) which is not suitable for unstable proteins. The separation of labelled protein from unlabelled molecules is also a necessary step for this technique.

1.6.2. Considerations on photo-Met PIER and its potential

As a newly defined technique photo-Met PIER should be able to offer unique possibilities and advantages in comparison to other conventional ET initiation approaches.

Unlike Re^{I} complexes PIER allows us to keep studied protein closer to its native structure and function since no bulky complex is introduced to the experiment. Photo-Met incorporation is specific and does not require additional residues like accessible His on the surface to anchor Re^{I} complex. Another major potential advantage is ability to introduce photo-Met and perform PIER experiment close to the active site deep inside the structure of a protein which is not feasible with Re^{I} complexes. On the other hand, when compared directly to Re^{I} labelling the glaring disadvantage of PIER becomes obvious – diazirine group of photo-Met is irreversibly lost after photoactivation and formation of reactive carben and can no longer be recovered, thus limiting us to only one experiment with specific sample. Since incorporation of photo analogue like photo-Met into protein sequence poses some challenges this can negatively affect the throughput of PIER as an ET research technique (level of photo analogue incorporation affects ET reaction yield), a problem which could, at least partially, be solved by iteration and optimisation of the experimental protocol.

After taking into account these considerations and our previously achieved results [43] we would claim that PIER shows promise and deserves further research, characterisation and comparative analysis to other ET initiation techniques.

2. Goals

For this thesis four major goals are defined.

- Expression of recombinant azurin (AzWT & Az2W mutant) in nutritionally rich LB medium and its purification.
- Incorporation of photo-Met into AzWT & Az2W sequence during expression in mineral medium M9 and purification of azurin with satisfactory photo-Met incorporation ratio.
- Study of azurin oligomerization and particularly effect of increasing azurin total concentration in solution on oligomers formation (primarily dimers) using photo-induced cross-linking.
- Characterization of photo-induced changes of redox state of Cu atom at azurin active site previously observed in photo-Met-containing azurins.

3. Materials

3.1. Chemicals

Tryptone (Bio Basic Canada)

NaCl (Fluka)

Yeast extract (Bio Basic Canada)

HCl (Fluka)

Na_2HPO_4 (Lach-Ner)

KH_2PO_4 (Lachema)

NH_4Cl (Lachema)

$MgSO_4$ (Sigma)

$CaCl_2$ (Fluka)

Ethylenediaminetetraacetic acid (EDTA) (Fluka)

$CoCl_2.6H_2O$ (Lachema)

$FeSO_4.7H_2O$ (Sigma)

$ZnSO_4 . 7H_2O$ (Sigma)

$CuSO_4.5H_2O$ (Lachema)

$MnCl_2.4H_2O$ (Sigma)

H_3BO_3 (Lachema)

Glucose (Sigma)

Thiamine hydrochloride (Sigma)

L-Ile (Sigma)

L-Val (Sigma)

L-Leu (Sigma)

L-Lys (Sigma)

L-Phe (Sigma)

L-Thr (Sigma)

L-Met (Sigma)

L-photo-Met (Thermo Scientific)

Trizma® base (Tris-Cl) (Sigma)

Glycerol (Lachema)

KCl (Lachema)

$MgCl_2$ (Lachema)

Ampicillin (Roth)

Isopropyl β-d-1-thiogalactopyranoside (IPTG) (Roth)

Sucrose (Penta)

Ammonium acetate (Lachema)

Acrylamide (Bio Rad)

Sodium dodecyl sulfate (SDS) (Sigma)

2-mercaptoethanol (Sigma)

Bromothymol blue (Roth)

Coomassie Brilliant Blue R-250 (Sigma)

Ammonium persulfate (Sigma)

Tetramethylethylenediamine (TEMED) (Fluka)

PageRuler™ Unstained Broad Range Protein Ladder (Thermo Scientific)

Precision Plus Protein™ Dual Color Standard (BioRad)

Acetic acid (Sigma)

Methanol (Lachema)

Formaldehyde (Sigma)

Ethanol, HPLC-grade (Merck)

Acetonitrile, HPLC-grade (Merck)

Water, HPLC-grade (Merck)

Ethylmorpholine (Sigma)

Tris(2-carboxyethyl)phosphine (TCEP) (Sigma)

Iodoacetamide (Sigma)

Trypsin protease (0,1 g/l solution, Promega)

Lys-C endoprotease (0,1 g/l solution, Roche)

Trifluoroacetic acid (TFA) (Fluka)

MALDI matrix (3 mg/ml α-cyano-4-hydroxycinnamic acid in 50% (v/v) acetonitrile and 0,1% (v/v) TFA) (Bruker Daltonics)

Bicinchoninic acid (BCA A) (Sigma)

4% solution of $CuSO_4.5H_2O$ (BCA B) (Sigma)

3.2. Equipment

Hoefer Mighty Small S260 Mini Vertical Protein Electrophoresis Unit

Laboratory pipettes and tips from Gilson and Eppendorf

Ohaus Discovery Analytical Balance

Ohaus Scout Pro Electronic Balance

DeNovix DS-11+ Spectrophotometer

Multiskan Bio Microplate Spectrophotometer (Thermo Scientific)

Oriel UV Light Source (PhotoMax Lamp Housing (60100-M), Arc Lamp Power Supply (68806-M), Electronic Safety Shutter (71445-M), Mercury Arc Lamp, 100 W (6281))

Hielscher UP100H Ultrasonic Homogenizer

Bandelin Sonopuls Ultrasonic Homogenizer with VS-70T probe

Incubator IKA® KS4000 iControl

Incubator Lab. Companion SI-600R

inoLab pH 7110 pH-meter with SenTix® 81 combination electrode (WTW)

Ultimate Dry Bath Incubator (Cleaver Scientific)

Hettich Zentrifugen Universal 320 R Centrifuge with 1620A angular rotor

Eppendorf miniSpin Plus Minicentrifuge

Labconco CentriVap®micro IR Vacuum Concentrator

MALDI-TOF Ultraflex III Mass Spectrometer (Bruker Daltonics)

Agilent UHPLC 1290 LC-MS system coupled with ESI-qTOF maXis PLUS Mass Spectrometer (Bruker Daltonics)

4. Methods

4.1. Recombinant azurin expression

To produce suitable amounts of azurin for other experiments we have applied an expression protocol which was previously optimised and described as part of the author's bachelor's thesis [43]. In the following text the most important major steps and further optimisations are described.

4.1.1. Medium preparation

All mediums used in expressions were prepared in-house.

For Met expression nutritionally rich Lysogeny Broth (LB) was prepared by dissolving 5 g of Tryptone, 5 g of NaCl and 2,5 g of yeast extract in approx. 450 mL of water. Medium was sterilised in autoclave after adjusting pH to 7,7 value with 5 M HCl and the final volume to 500 mL.

Mineral Medium M9 (MM-M9 or just M9) was used for expressions with L-photo-Met. Stock solutions for this medium include:

- 5× M9 pre-mix* – 42 mM Na_2HPO_4; 22 mM KH_2PO_4; 18 mM NH_4Cl; 8,6 mM NaCl
- 1 M $MgSO_4$*
- 0,1 M $CaCl_2$*
- 1000× metals mix** – 80,6 mM EDTA; 2,15 mM $CoCl_2.6H_2O$; 92,5 mM $FeSO_4.7H_2O$; 1,56 mM $ZnSO_4.7H_2O$; 13,5 mM $CuSO_4.5H_2O$; 10,6 mM $MnCl_2.4H_2O$; 1,62 mM H_3BO_3
- 20% (w/v) glucose**
- 1% (w/v) vitamin B_1 (thiamine hydrochloride)**
- 10× amino acids mix** – 0,5 mg/mL L-Ile, L-Val, L-Leu; 1 mg/mL L-Lys, L-Phe, L-Thr
- 50× L-photo-Met** – 1,5 mg/mL

* autoclave sterilisation, ** 0,22 μm filter sterilisation.

Table 3, p. 34 shows the amounts of each component required to prepare 100 mL of M9 medium.

Table 3 Preparation of 100 mL of M9 medium. After mixing the components (except photo-Met) according to the table adjust final volume with sterile dH_2O. Photo-Met should be added only after cells have adapted to M9 (see chapter 4.1.4, page 35).

Component	Volume (mL)
5× M9 pre-mix	20
1 M $MgSO_4$	0,5
0,1 M $CaCl_2$	0,1
1000× metals mix	0,1
20 % glucose	2
1% vitamin B_1	1
10× amino acids mix	10
50× L-photo-Met	2

4.1.2. Competent cells preparation

- Due to detrimental effect of Met on photo-Met incorporation during recombinant expression we have chosen *E. coli* strain B834(DE3)pLysS cells (Novagen, genotype: F^- *ompT hsdS*$_B$(r_B^- m_B^-) *gal dcm met* (DE3) pLysS (Cam^R)) which are methionine auxotrophs as our expression host.
- Inoculate small amount of commercial cell culture in LB medium and leave it to grow overnight at 37 °C and 180 RPM.
- The following day transfer 250 µL of overnight culture into 25 mL of fresh LB medium and leave to grow under the same conditions until optic density at 600 nm (OD600) has reached 0,5.
- Leave cells to rest on ice for 15-20 min (to stop cell division) and harvest *via* centrifugation (Hettich Universal 320R, angular rotor 1620A, 4 °C, 5000 RPM, 5 min).
- To turn cells into competent gently resuspend cell pellet in 10 mL ice-cold 100 mM $CaCl_2$ in 10 mM Tris-Cl, pH 7,4 on ice and incubate on ice for 10 min.
- Harvest competent cells by gentle centrifugation (Hettich Universal 320R, angular rotor 1620A, 4 °C, 2000 RPM, 10 min) and after decanting the supernatant resuspend cell pellet in 1 mL ice-cold 50 mM $CaCl_2$, 15% (v/v) glycerol in 10 mM Tris-Cl, pH 7,4.
- Use 100-200 µL aliquots of competent cells immediately for transformation or freeze them with liquid nitrogen and store at –80 °C.

4.1.3. Competent cells transformation with expression plasmid

- Transfect competent cells with expression plasmid including azurin cDNA (40–60 ng of plasmid per 50 µL of competent cell culture) using standard heat shock protocol: 90 seconds at 42 °C followed by 3-minute incubation on ice.

- Growth in 0,5 mL of SOC medium (2% (w/v) tryptone, 0,5% (w/v) yeast extract, 10 mM NaCl, 2,5 mM KCl, 10 mM $MgCl_2$, 10 mM $MgSO_4$, 20 mM glucose) with no antibiotic for 1 hour at 37 °C and 180 RPM.
- Transfer and spread 100 µL of cell culture on agar plates with 100 µg/ml ampicillin final concentration (amp_{100}) to provide selection pressure.
- Incubate agar plates at 37 °C overnight in bottom-up position.
- Evaluate the plates and store successfully transformed cells at 4 °C in the darkness with parafilm cover. Cells prepared in this manner can be stored for about a month.

4.1.4. Expression in rich LB and limited M9 media

- Inoculate one colony from a plate in 20–30 mL of LB medium, amp_{100} and incubate at 37 °C and 180 RPM overnight.
- Determine OD600 (measurement in 3–5× diluted sample) of overgrown overnight culture and transfer a small amount to 150 mL of LB medium, amp_{100} in 500 mL Erlenmeyer flask.
- The amount of used overnight culture is assigned based on its OD600 so resulting OD600 is ~0,05 after inoculation.
- Incubate cells at 37 °C and 180 RPM until OD600 reaches value ~0,6.
    - For photo-Met azurin expression wash cells with PBS (Phosphate Buffered Saline; 10 mM Na_2HPO_4, 1,8 mM KH_2PO_4, 137 mM NaCl, 2,7 mM KCl, pH 7,4) three times and gently resuspend cell pellet in limited M9 medium, amp_{100}.
    - To harvest cells and remove LB medium (or used PBS) centrifugate cells (Hettich Universal 320R, angular rotor 1620A, 4 °C, 5000 RPM, 15 min) and decant supernatant.
    - Once cells have adapted to M9 medium (after 15–20 min incubation) add photo-Met (final concentration 30 mg/L) and give them another 15–20 min to adapt and intake photo-Met.
    - For Met azurin expression in LB medium no PBS wash steps, or photo-Met addition, are required.
- To initiate azurin expression add IPTG (isopropyl-β-D-1-thiogalaktopyranosid, final concentration 0,6 mM)
- Incubate cells at 30 °C (to reduce photo-Met degradation and facilitate slower protein expression both of which help increase photo-Met incorporation) and 180 RPM for 18–20 hours.
- After expression is completed incubate cells on ice for 10 min and harvest *via* centrifugation (Hettich Universal 320R, angular rotor 1620A, 4 °C, 5000 RPM, 20 min).
- To facilitate osmotic shock as first step of azurin isolation resuspend cell pellet in 40 mL of 20 % (w/v) sucrose solution (20 mM Tris-Cl and 1 mM EDTA, pH 8,1) and incubate at room temperature for 30 min.

- Centrifugate the cells (Hettich Universal 320R, angular rotor 1620A, 4 °C, 9000 RPM, 20 min) to remove sucrose solution and freeze pellets at –20 °C. Cell pellets with overexpressed recombinant azurin prepared in such way can be stored for several months.

4.2. Recombinant azurin purification

Same as with expression, azurin isolation approach has also been previously optimised. The protocol is shown as a block-scheme on Figure 11.

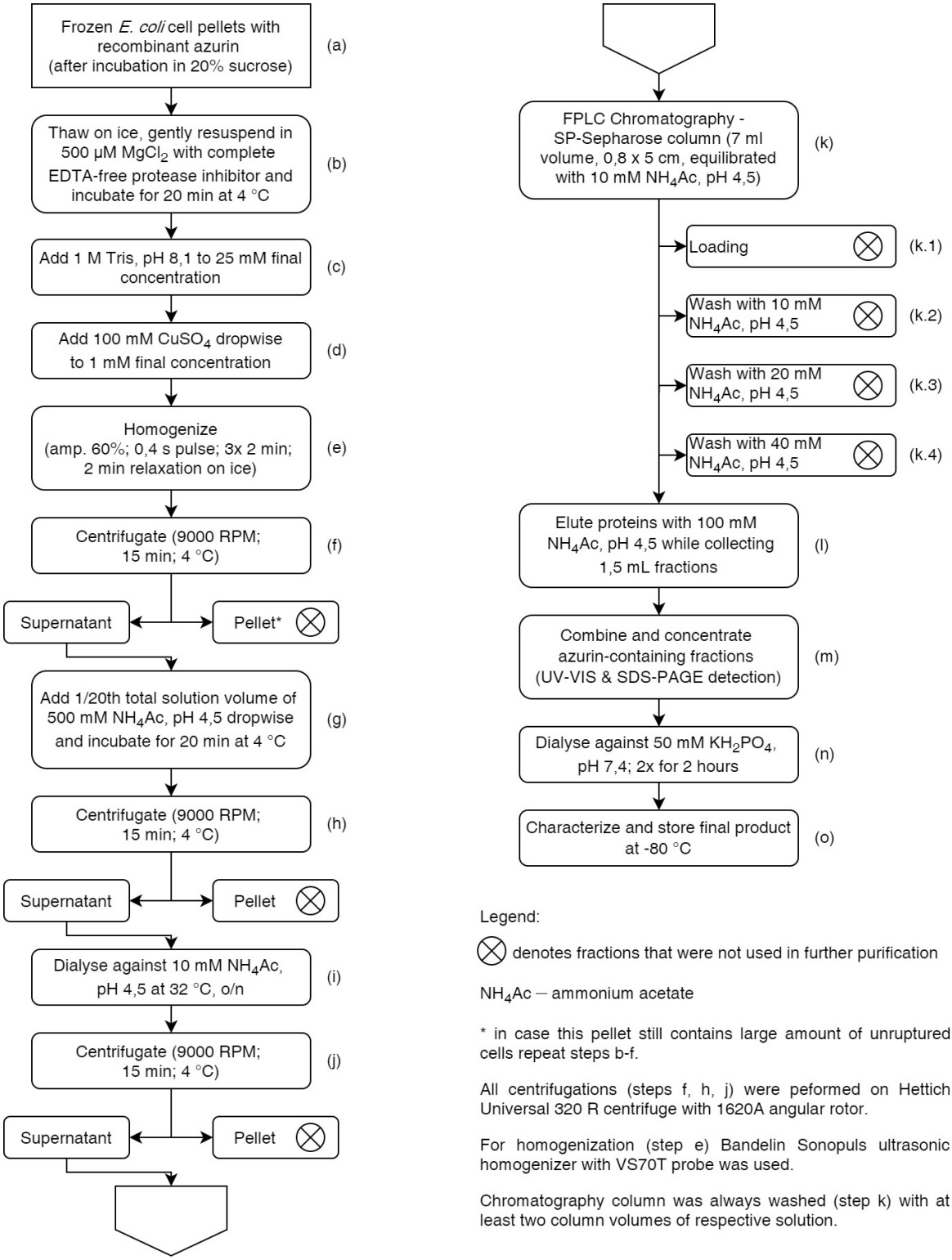

Figure 11 Detailed scheme of azurin purification**.**

4.3. Mass Spectrometry (MS) experiments

An extremely powerful analytical method for modern biochemistry – mass spectrometry – utilises different behaviour of charged particles of ionized sample in electromagnetic field to detect signals in the form of mass/charge (*m/z*) ratios. To prevent alterations of trajectory of ions and molecules of the analysed compound, analysis and detection are performed in high vacuum.

To ionize and transfer a biochemical sample into gas phase one of the two main techniques is usually chosen. In ElectroSpray Ionisation (ESI) a liquid sample (e.g. on-line coupled liquid chromatography – LC-MS) is ionized by high voltage at the tip of spraying capillary and transferred to high vacuum through heated capillary by differential vacuum pumping system. Another commonly employed ionization method is Matrix Assisted Laser Desorption Ionization (or MALDI). In this approach a sample is mixed with a matrix compound (for UV lasers usually a small organic aromatic acid) in a $1{:}10^4$ ratio. Molecules of matrix are capable of photon absorption followed by desorption together with the analyte after laser irradiation. During this process a proton transfers to/from the analyte molecule resulting in its ionization. MALDI is particularly useful for analysis of complex samples since it prevalently produces single-charged ions of $[M–H]^-$ or $[M+H]^+$ types.

The most common and accessible analysers used in biochemical MS are Time Of Flight (TOF) and Quadrupole (q). As the name implies, TOF analyser measures the time it takes for ions which were given the same acceleration per unit of charge to reach the detector. Light ions with low *m* will arrive at the detector first and *vice versa*. In a quadrupole analyser (formed by four quadrupole rods), ions are separated based on the stability of their trajectories in oscillating radiofrequency electric fields which are applied sequentially to two opposite rods. The most modern approaches to biochemical MS offer unrivalled precision and accuracy and employ novel analysers like Orbitrap or FT-ICR (Fourier Transform Ion Cyclotron Resonance).

4.3.1. In-gel protein digest and MS determination of photo-Met incorporation ratio

Relative incorporation of analogous amino acid into the sequence of a protein can be determined using MS. Peaks corresponding to peptides containing an analogue (either intact in case of ESI or as a termination product when the samples are measured after photoactivation (by 350−370 nm UV light) or MALDI (with N_2-laser, 337 nm) is employed) can be identified and distinguished on MS spectrum due to the difference in mass of an intact/termination product of analogue and a native amino acid (in case of photo-Met difference for native amino acid/termination product pair is −19,972 m.u., for native amino acid/intact analogue it is +8,034 m.u., see Figure 12, p. 39). The incorporation ration can then be determined by comparing areas under curve for monoisotopic *m/z* signals.

$$photo\text{-}Met\ incorporation\ ratio = \frac{S(photo\text{-}Met)}{S(Met) + S(photo\text{-}Met)} \cdot 100\%$$

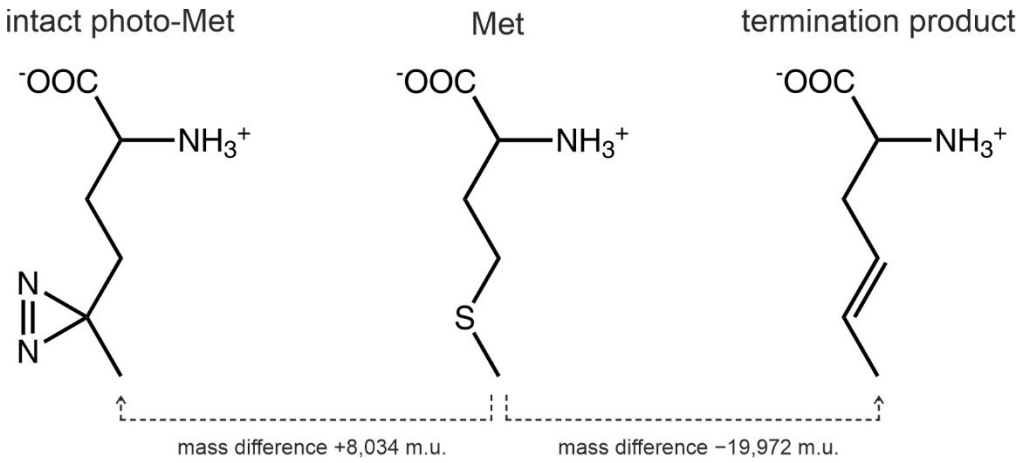

Figure 12 Structures of native Met, intact photo-Met and its termination product. Mass difference between the pairs allows to distinguish photo-Met-containing peptides in MS spectrum from their Met counterparts and determine photo-Met incorporation.

In all cases we have used sodium dodecyl sulfate polyacrylamide gel electrophoresis (SDS-PAGE) with Coomassie Brilliant Blue R-250 (CBB R-250) visualisation to perform the initial separation and evaluation of a protein sample. The protocol we have used was previously described [43].

To prepare the samples for MS we have performed an in-gel proteolytic digest of studied proteins. Gel bands corresponding to target proteins were excised using a scalpel and cut into small pieces. To remove CBB R-250 gel pieces were submerged in approx. 150 µL of 50 mM ethyl morpholine buffer, pH 8,1 (EtMf) in 50% (v/v) acetonitrile (ACN) and incubated in a sonication bath until de-stained. The samples were then rinsed with 100 µl of ACN. To reduce S-S bridges samples were incubated in 30 mM solution of tris(2-carboxyethyl)phosphine (TCEP) in 100 mM EtMf, pH 8,1 for 15 minutes at 70 °C. To remove TCEP sample were then once again rinsed with 100 µL of ACN. To prevent re-forming of disulfide bridges from reduced cysteine residues, their modification by 1-hour incubation in 30 mM iodoacetamide (IAA) in 100 mM EtMf, pH 8,1 in the darkness was performed. After the modification IAA solution was removed by rinsing in ACN and the samples were additionally rinsed with 100 µL of water, ACN, water and finally 50% (v/v) ACN in water. Samples were then dried out using Labconco CentriVap® micro IR. To perform the digest, proteolytic mix (1 µL of trypsin (0,1 g/L) or other endoprotease in 40 µL of proteolytic buffer (50 mM EtMf, pH 8,1, 10% (v/v) ACN)) was added to cover gel pieces and samples were incubated at 37 °C overnight.

Protease activity was stopped by addition of ACN (40% (v/v) final concentration) and trifluoroacetic acid (TFA, 0,1% (v/v) final concentration) which simultaneously facilitated

extraction of peptides from the gel. After 15 minutes of sonication 0,4 μL of sample were transferred onto a MALDI target plate for MALDI-TOF MS analysis. The dry spot of sample on the plate was overlaid with 0,4 μL of matrix solution (3 mg/mL α-cyano-4-hydroxycinnamic acid in 50% (v/v) ACN and 0,1% (v/v) TFA). MS spectra were acquired on Bruker Daltonics Ultraflex III MALDI-TOF mass spectrometer under supervision of doc. RNDr. Miroslav Šulc, Ph.D.

4.4. Photo-induced cross-linking experiments

Azurin samples with satisfactory protein concentration and photo-Met incorporation ratio were analysed in PIXL experiments. Samples of Met azurin were used as controls.

The UV light source used in the experiments was produced by Oriel (see chapter 3.2, p. 32). The samples were illuminated in a quartz capillary which was submerged in a Pyrex glass cuvette with water. Water in this setup ensured sufficient heat transfer from the samples to cooled cuvette holder and Pyrex glass was used to shield the samples from destructive short wavelength (< 280 nm) UV. Based on our previous finding's illumination time was kept to one minute. UV-Vis spectra of the samples were measured before and immediately after illumination and dilution to similar final concentration of azurin using DeNovix DS-11+ spectrophotometer. Since measurements were performed in microvolume, each sample was measured in triplicates. Visualization and separation of formed cross-linked products was performed employing 15% SDS-PAGE.

5. Results

5.1. Follow the blue, recombinant azurin expression and purification

Since expression (in both LB and MM-M9) and purification of recombinant azurin and their respective optimisation were discussed in detail in the author's bachelor's thesis [43] this chapter will only include several illustrative intermediate results, novel findings and detailed characterization of final proteins which were used in further experiments.

5.1.1. Azurin expression, comparison between MM-M9 and DMEM-LM

Our previous results have shown that after 16–18 hours azurin expression with Met in M9 medium is not significantly hindered compared to expression in LB. To expand on this, we have compared azurin expression with photo-Met in in-house prepared M9 medium (see chapter 4.1.1, p. 33) and commercially available Dulbecco's Modified Eagle Limiting Medium (DMEM-LM) from Thermo Scientific (4,5 g/L glucose, 4,0 mM L-Gln, sodium pyruvate) designed for photo-Met incorporation. Additionally, in this experiment we have tried extending expression time to twenty-four hours.

The experiment was performed on a smaller scale, with only 10 mL of medium in 50 mL plastic Falcon® conical tubes, but otherwise following the protocol outlined in chapter 4.1.4, p. 35. A colony of *E. coli* B834(DE3)pLysS cells transformed with expression plasmid carrying azurin cDNA (chapter 4.1.3, p. 34) the previous day was inoculated in 20 mL LB, amp_{100} and incubated for 4,5 hours at 37 °C, 180 RPM until OD600 has reached 0,583. After that, cells were harvested according to the described method and washed 4× with 15 mL of PBS. On the last wash cycle cell suspension was split in halves and after removal of PBS one of the resulting cell pellets was resuspended in 10 mL of M9, amp_{100} and the other in 10 mL of DMEM-LM, amp_{100}. Following the protocol, photo-Met and IPTG were added to the medium (to 30 mg/L and 0,6 mM final concentration, respectively) and expression was performed at 30 °C, 180 RPM for 24 hours. To prepare samples for SDS-PAGE, 500 µL of cell culture were taken from each tube at 0 (just before the addition of IPTG), 1, 18 and 24 hours, and after centrifugation (Eppendorf miniSpin Plus, 14500 RPM, 2 min) supernatants were removed and cells were resuspended in 40 µL of sterile dH_2O and stored at −20 °C. Before loading on SDS-PAGE 10 µL of 5× concentrated loading buffer was added to each sample and 10 min incubation at 98 °C was performed together with sample homogenization employing Hielscher UP100H ultrasonic homogenizer, 60% amplitude, 3× 20 s pulse.

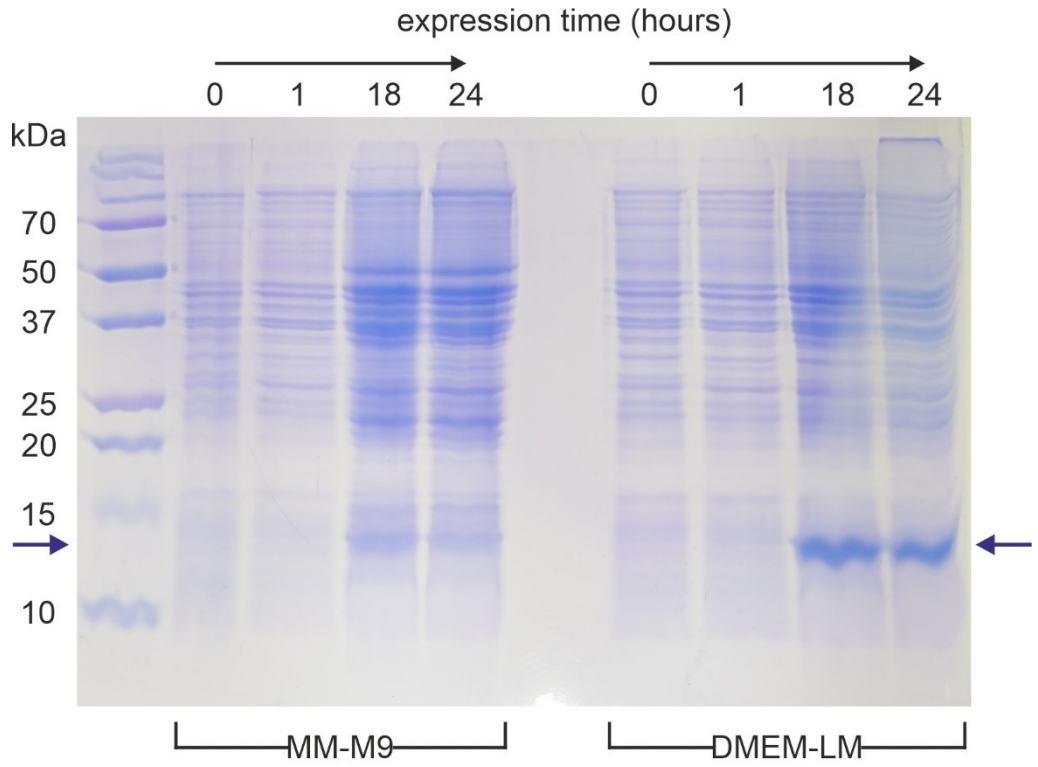

Figure 13 15% polyacrylamide electrophoretic gel with protein bands visualised with CBB-R250 showing the comparison between twenty-four-hour azurin expression in "in-house" MM-M9 and commercially available DMEM-LM. Blue arrows depict relative mobility of azurin. Despite lower total amount of azurin in MM-M9, photo-Met incorporation ratio is significantly improved under these conditions. This general trend is commonplace when proteins with photo-Met are produced – lower total protein amount correlates with higher photo-Met incorporation.

As Figure 13 shows, the expression was successful in both media. Total amount of azurin produced (protein band with MW of approx. 14 kDa, see position of blue arrows) in DMEM-LM was higher than in MM-M9. Despite this seeming advantage of DMEM-LM, after azurin bands were excised from the gel, enzymatically digested with trypsin and analysed employing MALDI-TOF MS (see protocol in chapter 4.3.1, p. 38) significantly lower photo-Met incorporation ratio in DMEM-LM compared to in-house prepared M9 medium was revealed as illustrated in Table 4.

Table 4 Photo-Met incorporation ratio in different peptides of Az2W expressed for 18 hours in DMEM-LM and MM-M9 determined by MALDI-TOF MS after trypsin in-gel digest. The results for the second colony arise from a second identical experiment and show that colony selection has minimal influence on photo-Met incorporation.

Sample	Medium	Relative photo-Met incorporation (%)	
Detected *m/z* signal $[M+H]^+$		3056,4051	2698,2089
Peptide sequence: **Az2W**		104-128	1-24
Colony 1	DMEM-LM	1	5
Colony 1	MM-M9	14	25
Colony 2	DMEM-LM	1	2
Colony 2	MM-M9	14	25

Corroborating with our previous results, nearly no azurin has been produced in the cells after one hour. Extending expression time to twenty-four hours resulted in slight reduction in total amount of expressed azurin in the samples (see protein band intensity on Figure 13, p. 42) with no noticeable change to photo-Met incorporation ratio compared to eighteen-hour expression based on MALDI-TOF MS.

5.1.2. Tried and tested, azurin purification

Compared to version of the protocol for recombinant azurin purification we have published earlier several minor improvements have been introduced. Addition of Tris-Cl buffer to cell lysate (step (c) on Figure 11, p. 37) prevented premature azurin precipitation by $CuSO_4$ added in the following azurin metalation step. Instead of time-consuming titration with 100 mM $CuSO_4$ with UV-Vis detection in step (d) (on Figure 11, p. 37) we have moved to direct addition of $CuSO_4$ to 1 mM final concentration.

A record of a representative azurin purification is shown on Figure 14, p. 44. All of the bulk proteins from crude cell lysate are successfully removed during the process and final chromatography fractions contain pure azurin.

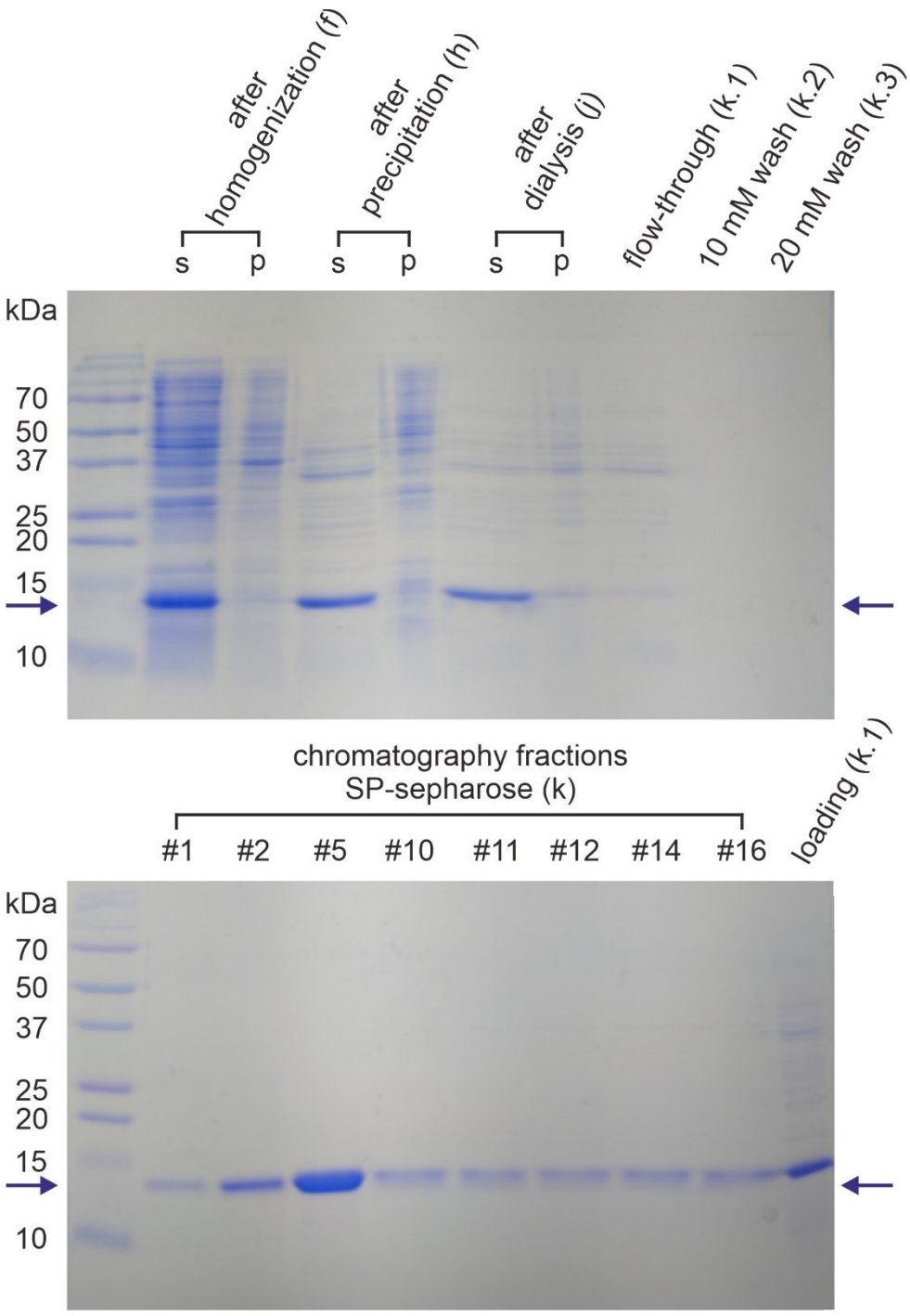

Figure 14 15% polyacrylamide electrophoretic gels with protein bands visualised with CBB-R250 recording one of the performed azurin purifications. **Top** – samples from early stages of purification (cell homogenization, bulk protein acid precipitation). **Bottom** – record of FPLC chromatography on SP-Sepharose column (the numbers mark corresponding fractions during elution with 100 mM NH_4Ac, pH 4,5). Blue arrows depict relative mobility of azurin. Samples for SDS-PAGE were taken after every centrifugation, where applicable, supernatants are marked with **s** and pellets with **p**. All pellets were diluted 20× before being loaded on gel. Letters in brackets refer to steps described in the flowchart of purification protocol on Figure **11** in chapter 4.2, p. 37.

5.1.3. Characterization of final products

In the scope of this study we have focused on comparing the behaviour of wild type azurin (AzWT) and azurin mutant H83Q K122W T124W T126H All-Phe (Az2W).

Using expression and purification protocols described above we have prepared azurins with photo-Met in the sequence and controls with Met to use in the experiments. After isolation final products were characterized by measuring their UV-Vis spectra (specifically A_{280} and A_{630} values), protein concentration evaluation using BCA assay (bicinchoninic acid, the protocol was described earlier [43]) and (where applicable) MALDI-TOF MS to determine photo-Met incorporation. The resulting values are summarized in Table 5 and Table 6.

Table 5 Characterization of azurin final products. Molar concentrations listed are based on $\varepsilon_{630} = 5700\ M^{-1}\ cm^{-1}$ for azurin. Total protein mass concentrations were determined by BCA assay using 0,1–1 mg/mL BSA as standard protein.

Protein	A_{280}	A_{630}		A_{630}/A_{280}	c (mM)	ρ (mg/mL)
AzWT Met	3,6	0,73	(10× dil.)	0,20	1,28	10,4
AzWT photo-Met	2,4	1,2	(5× dil.)	0,50	1,05	8,40
Az2W Met	1,40	0,45	(10× dil.)	0,32	0,80	9,45
Az2W photo-Met	0,84	0,32	(10× dil.)	0,38	0,56	7,41

Table 6 Photo-Met incorporation ratio in different peptides of AzWT and Az2W final products determined by MALDI-TOF MS. Results marked with "–" denote that respective peptide was not detected in the spectrum.

Sample		Relative photo-Met incorporation (%)			
Theoretical *m/z* signal $[M+H]^+$		2279,9928	2698,2089	3004,3967	4093,9058
Peptide sequence: **AzWT**		104-122	1-24	42-70	42- 79
Protease	Trypsin	40	51	–	37
	Lys-C	33	45	35	–
Theoretical *m/z* signal $[M+H]^+$		3056,4051	2698,2089	2965,3858	4038,9000
Peptide sequence: **Az2W**		104-128	1-24	42-70	42- 79
Protease	Trypsin	–	12	–	22
	Lys-C	–	10	19	–

5.2. Photo-induced processes, more than just cross-links

As part of author's bachelor's thesis, we have previously performed several successful PIXL experiments with azurin. In that study, we have focused primarily on the effect of ionic strength of the solution on azurin oligomerization and have found that increasing salt concentration has a detrimental effect on azurin dimer formation. This finding has led us to believe that ionic bonds are at least partially responsible for the interaction on the contact surface between two azurin molecules in dimer.

More than that, we have noticed an intriguing decrease of A_{630} value (which correlates with reduction of Cu(II)-azurin) after UV irradiation of photo-Met-containing AzWT. To test our hypothesis and confirm the role of photo-Met in this process we have performed the same experiment with AzWT with Met where A_{630} value decrease was also observed but on a much lower scale. We have attributed this minor decrease to potential effect of W (specifically one in position 48 in azurin, since it lies in close vicinity of the active site), which is also known to form reactive intermediates after UV light irradiation. Because of that, as our last control we have also studied All-Phe mutant of azurin (as was described before, all naturally occurring W and Y replaced with F) with Met. In this protein, in absence of both Trp and photo-Met nearly no A_{630} decrease was observed.

In this work we have decided to explore the effect of protein concentration on azurin oligomerization to expand on our previous findings. Additionally, after seeing the potential application of photo-Met as a source of electrons for an ET process, we have also carefully studied UV-Vis spectra of the samples and employed Az2W mutant, in which abnormally high rates of ET were previously reported [42].

5.2.1. Azurin dimers can be linked by photo-Met

Azurin samples with a range of different protein concentrations (here and therefore, determined based on $\varepsilon_{630} = 5700\ M^{-1}\ cm^{-1}$ value for azurin) were exposed to intense UV irradiation in the setup described in chapter 4.4, p. 40. PIXL experiments were performed with 15, 35, 50, 150 and 300 μM samples of photo-Met-containing AzWT and Az2W. All measurements were performed in 50 mM KH_2PO_4, pH 7,4 to allow comparison of our findings with literature [41]. The amount of formed cross-links was estimated based on intensity of protein band on SDS-PAGE (all samples were diluted to 15 μM before loading on gel). Moreover, protein moiety of observed bands (since azurin has MW of approx. 14 kDa its dimers were expected to have relative mobility corresponding to a 28–30 kDa protein) was analysed in a top-down approach *via* MALDI-TOF MS after in-gel enzymatic digestion.

Same as in previous experiments cross-linked azurin dimers (di) were observed on SDS-PAGE (Figure 15, p. 47), with intensity of their corresponding protein band increasing with total azurin concentration in the sample.

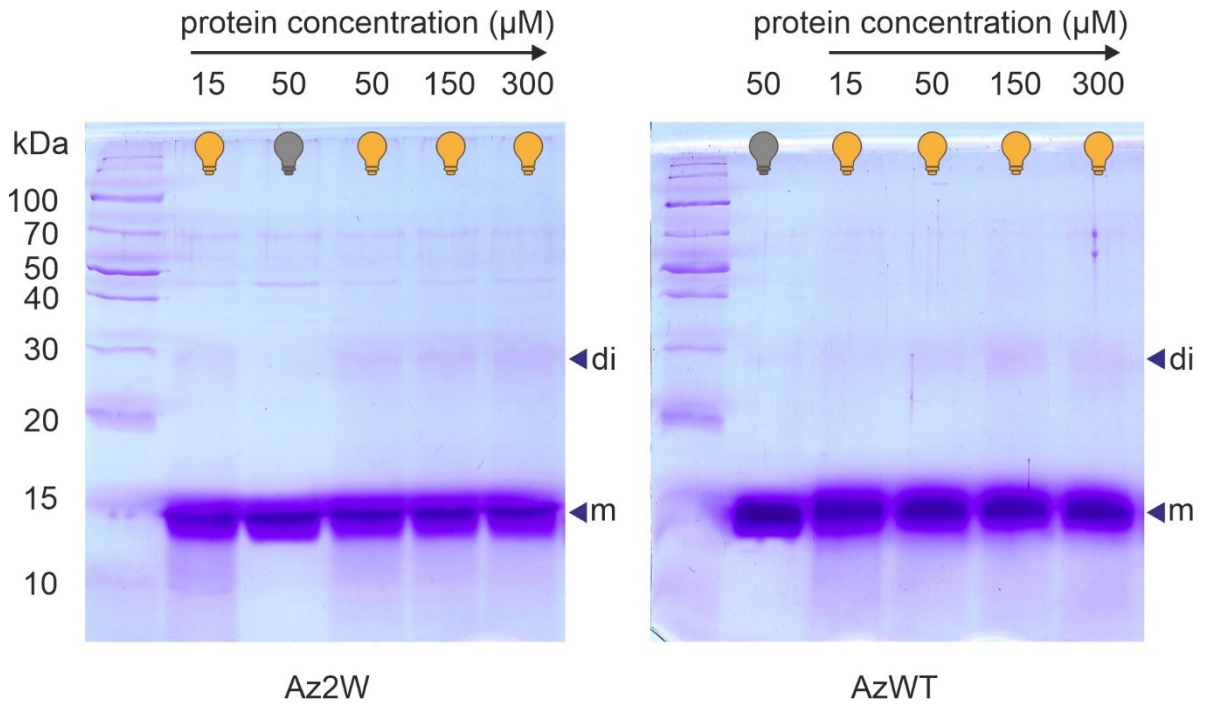

Figure 15 15% polyacrylamide electrophoretic gel with protein bands visualised with CBB-R250 showing the results of PIXL experiment with photo-Met-containing AzWT (35−50% photo-Met incorporation, **right**) and Az2W construct (10−20% photo-Met incorporation, **left**). Total concentration of azurin during PIXL experiment in each sample is listed at the top. All samples were diluted to 15 μM total azurin concentration before being loaded on gel. The samples which were exposed to UV light are depicted by a lit lamp symbol, control non-irradiated samples with a dark lamp. The position of letters to the right corresponds with relative mobility of monomeric azurin (m) and azurin dimer (di). The intensity of dimers increases with protein concentration, at the same time it is overall slightly lower in AzWT compared to Az2W.

When compared, AzWT and Az2W show a noticeable difference in behaviour.

In AzWT bands corresponding to dimer are very light when total azurin concentration is low and only begin to noticeably stand out in 50 μM sample. On the other hand, in Az2W cross-linked dimer can be observed even in 15 μM sample, the lowest concentration we have studied (see Figure 15 and Figure 16, p. 48). This effect is particularly noticeable when low concentration samples (15, 35 and 50 μM) are compared side by side on Figure 16, p. 48.

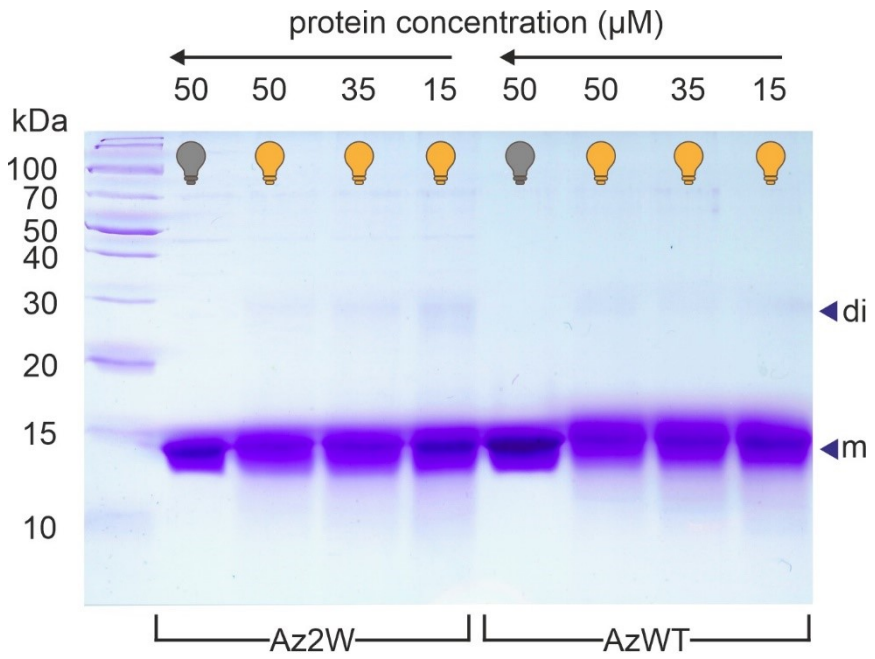

Figure 16 15% polyacrylamide electrophoretic gel with protein bands visualised with CBB-R250 showing the results of PIXL experiment with photo-Met-containing AzWT and Az2W construct at lower concentrations (35−50% and 10−20% photo-Met incorporation, respectively). Total concentration of azurin during PIXL experiment in each sample is listed at the top. All samples were diluted to 15 μM total azurin concentration before being loaded on gel. The samples which were exposed to UV light are depicted by a lit lamp symbol, control non-irradiated samples with a dark lamp. The position of letters to the right corresponds with relative mobility of monomeric azurin (m) and azurin dimer (di). Protein bands corresponding to Az2W dimer are more pronounced than those of AzWT.

Following the top-down approach we have utilised MALDI-TOF MS analysis of enzymatically digested (trypsin and Lys-C) cross-linked monomers dimers to confirm the identity of those protein bands as azurin moieties. Sequence coverage for AzWT, together with illustrative MS spectra of monomeric and dimeric azurin forms are shown on Figure 17, p. 49 and Figure 18, p. 49, respectively.

On both spectra the enlarged area shows *m/z* range corresponding to C-terminal peptide (2279,9928 theoretical *m/z*, amino acids 104−122). Photo-Met incorporation ratio for this peptide can be calculated from the monomer spectrum (see chapter 4.3.1, p. 38). Peak with 2279,905 m/z corresponds to the monoisotopic mass of peptide with two Met, 2259,918 m/z is a peptide with one Met and one photo-Met and finally 2239,941 m/z is the signal of peptide with two photo-Met. Area under curve of those peaks can be used to determine relative photo-Met incorporation ratio (see also Table 6, p. 45). In dimer spectrum the enlarged area explains the absence of *C-termini* of the protein in sequence coverage (Figure 17, p. 49). As is obvious from them spectrum, no *m/z* signal corresponding to this peptide was detected.

monomer AzWT/trypsin [Protein sequence coverage: 87%]

```
  1 AECSVDIQGN DQMQFNTNAI TVDKSCKQFT VNLSHPGNLP KNVMGHNWVL
 51 STAADMQGVV TDGMASGLDK DYLKPDDSRV IAHTKLIGSG EKDSVTFDVS
101 KLKEGEQYMF FCTFPGHSAL MKGTLTLK
```

dimer AzWT/trypsin [Protein sequence coverage: 71%]

```
  1 AECSVDIQGN DQMQFNTNAI TVDKSCKQFT VNLSHPGNLP KNVMGHNWVL
 51 STAADMQGVV TDGMASGLDK DYLKPDDSRV IAHTKLIGSG EKDSVTFDVS
101 KLKEGEQYMF FCTFPGHSAL MKGTLTLK
```

monomer AzWT/Lys-C [Protein sequence coverage: 80%]

```
  1 AECSVDIQGN DQMQFNTNAI TVDKSCKQFT VNLSHPGNLP KNVMGHNWVL
 51 STAADMQGVV TDGMASGLDK DYLKPDDSRV IAHTKLIGSG EKDSVTFDVS
101 KLKEGEQYMF FCTFPGHSAL MKGTLTLK
```

dimer AzWT/Lys-C [Protein sequence coverage: 44%]

```
  1 AECSVDIQGN DQMQFNTNAI TVDKSCKQFT VNLSHPGNLP KNVMGHNWVL
 51 STAADMQGVV TDGMASGLDK DYLKPDDSRV IAHTKLIGSG EKDSVTFDVS
101 KLKEGEQYMF FCTFPGHSAL MKGTLTLK
```

Figure 17 MALDI-TOF MS peptide *m/z* signal azurin sequence coverage for SDS-PAGE bands corresponding to monomer and dimer in AzWT samples proteolytically cleaved with trypsin and Lys-C. Nearly full coverage was achieved in both monomer and dimer.

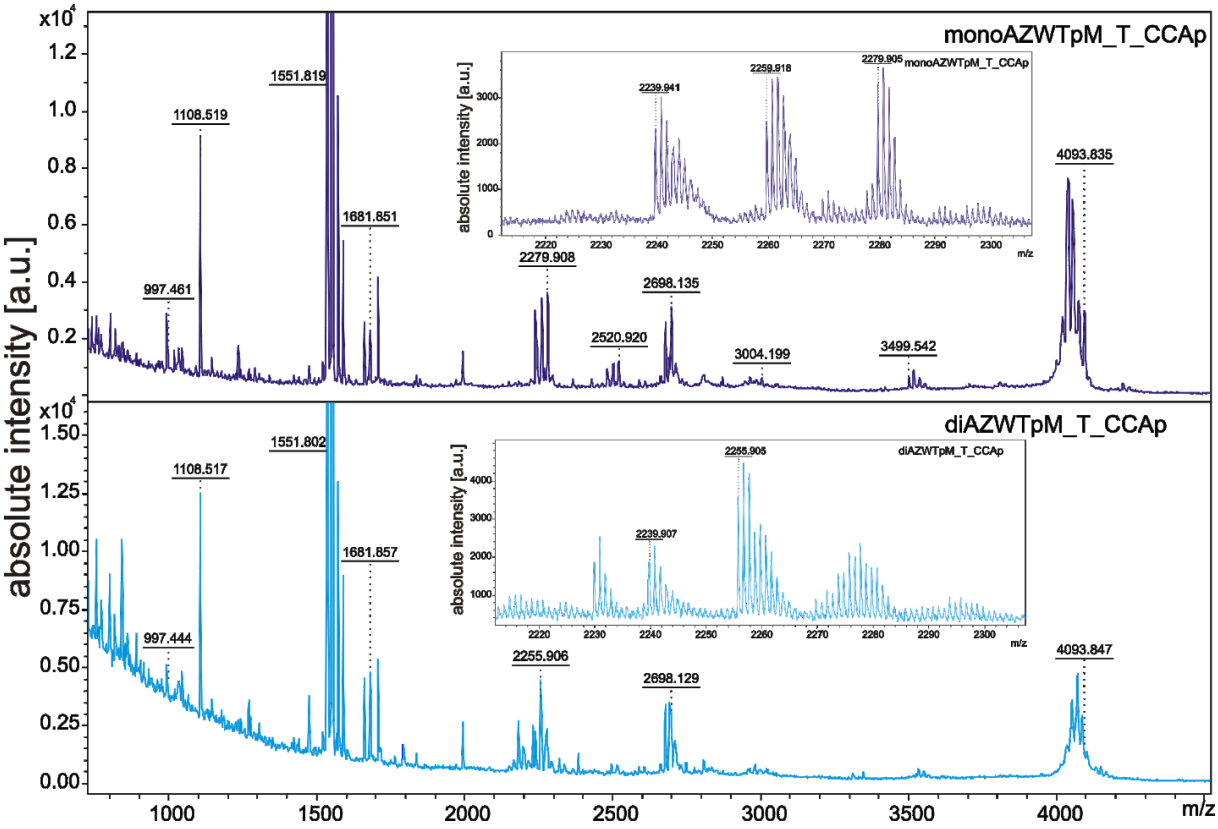

Figure 18 An illustrative MALDI-TOF MS spectra of monomer (**top, blue**) and dimer (**bottom, cyan**) AzWT samples cleaved with trypsin. In the monomer spectrum enlarged illustrates peptides which reveal photo-Met incorporation ratio. The peak with 2279,905 *m/z* corresponds to the monoisotopic mass of peptide with two Met, 2259,918 *m/z* is a peptide with one Met and one photo-Met and finally 2239,941 *m/z* is the signal of peptide with two photo-Met. Area under curve of those peaks can be used to determine relative photo-Met incorporation ratio (see chapter 4.3.1, p. 38).

In Az2W samples 97% and 60% sequence coverage was achieved for monomer and dimer, respectively, for samples digested with trypsin. When Lys-C was used the coverage was 77% for monomer and 64% for dimer.

We have also employed LC-MS/MS protocol on an ESI-qTOF system to map the cross-link in the observed dimer after trypsin in-gel proteolysis, but no additional *m/z* signals were detected on MS spectrum of dimer compared to monomer.

As our control, the protocol for PIXL was also carried out on AzWT and Az2W with Met in the structure. We have prepared 20, 60 and 120 µM samples of both of those proteins and have exposed them to UV light under the same conditions as in case of photo-Met azurins. Unsurprisingly, SDS-PAGE (all samples were diluted to 10 µM concentration before being loaded on gel, Figure 19) has revealed that no cross-links were formed in this experiment.

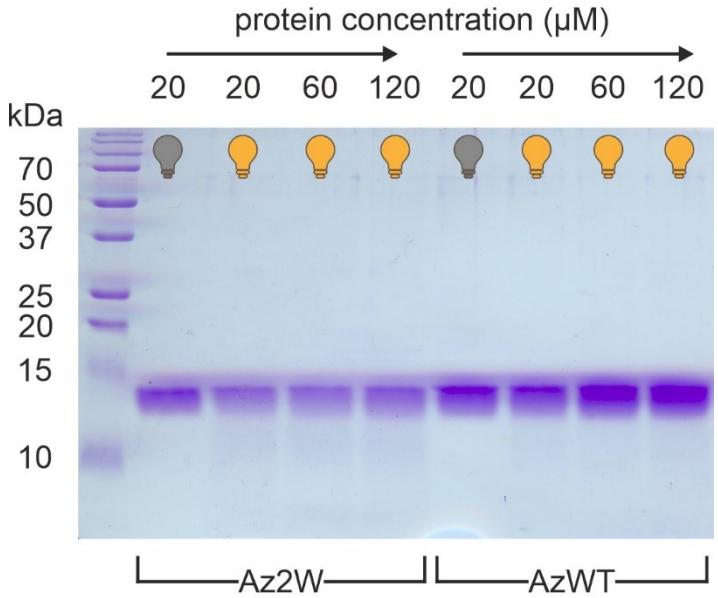

Figure 19 15% polyacrylamide electrophoretic gel with protein bands visualised with CBB-R250 showing the results of control PIXL experiment with Met-containing AzWT and Az2W construct. Total concentration of azurin during PIXL experiment in each sample is listed at the top. All samples were diluted to 10 µM total azurin concentration before being loaded on gel. The samples which were exposed to UV light are depicted by a lit lamp symbol, control non-irradiated samples with a dark lamp. As is obvious from the figure, no cross-links are observed in any of the samples.

5.2.2. Activated photo-Met induces changes in redox state of azurin

It is worth reiterating, that our earlier results suggested that photoactivation of azurin samples leads to decrease in A_{630} value. As we have found out, a minor component of this observation arises from the effect of W in the sequence (as was proven in control experiments with Met azurin and All-Phe mutant) but a much more significant role in the process can be attributed to the presence of photo-Met since it forms a highly reactive intermediate after UV irradiation which consequentially releases an electron and transfers it to a donor in protein structure. In this way photo-Met can potentially serve as a photoinducible initiator of ET reaction.

To acquire further insight into this process, as part of the PIXL experiments UV-Vis spectra of samples with increasing total azurin concentration were measured before and after photoactivation. For this measurement 150 and 300 μM samples of photo-Met AzWT and Az2W were diluted 3× and 6×, respectively, to allow better comparison of A_{630} value between particular samples and prevent it from going into spectrophotometer's non-linear response range (above 1,0 value of absorbance).

The same as in case of our previous findings, a decrease of A_{630} value which correlates with change of central Cu atom redox state in azurin active site was observed. This decrease exhibits similar trend as intensity of dimer band on SDS-PAGE and increases with total azurin concentration in a sample. In AzWT (35−50% photo-Met incorporation) A_{630} has decreased by 42 ± 7,4%, 44 ± 4,5% and 54 ± 1,7% after UV exposure in 50, 150 and 300 μM samples respectively. Most likely due to lower photo-Met incorporation ratio in Az2W (10−20% photo-Met incorporation) somewhat lower decreases of 15 ± 4,4%, 14 ± 1,1% and 21 ± 1,0% were observed (same as before, in 50, 150 and 300 μM azurin respectively). Listed values are based on three repeated experiments with six UV-Vis measurements for each sample in every one of them. These results are illustrated on Figure 20, p. 52 where spectra of individual samples from one of the experiments are shown. Full lines denote spectra of samples before UV irradiation, spectra after photoactivation are represented by dotted lines. For the sake of clarity of image, only part of the full spectrum between 500 and 750 nm is shown.

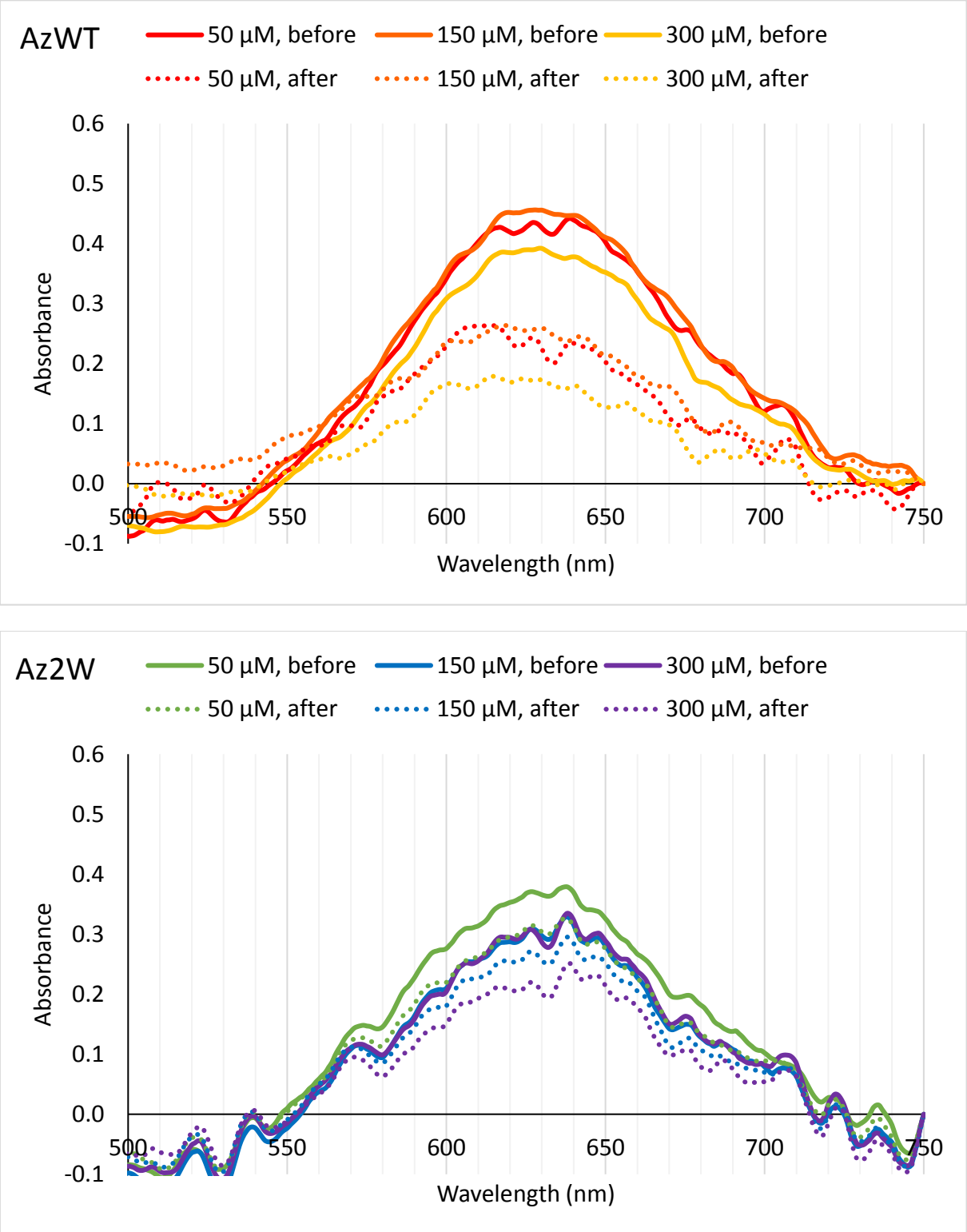

Figure 20 UV-VIS spectra of AzWT photo-Met (35−50% incorporation, **top**) and Az2W photo-Met (10−20% incorporation, **bottom**) samples before and after photoactivation measured in one of the PIXL/PIER experiments. Full lines – spectra before UV exposure, dotted lines – spectra after UV exposure. Enlarged area of the plot from 500 to 750 nm is shown.

Same as with PIXL experiments, Met-containing AzWT and Az2W were used as controls. For the same reasons as in case of photo-Met azurins 60 and 120 µM samples were also diluted 3× and 6× respectively before UV-Vis measurement.

As Figure 21 shows, in the absence of photo-Met A_{630} value in samples exhibits only minimal fluctuations within just a couple percent after UV exposure. Spectra for the highest studied 120 µM protein concentration, where the highest A_{630} decrease (approx. 5–8 % for both AzWT and Az2W) was observed, are shown. Under lower protein concentrations spectra before and after UV irradiation are nearly indistinguishable from each other.

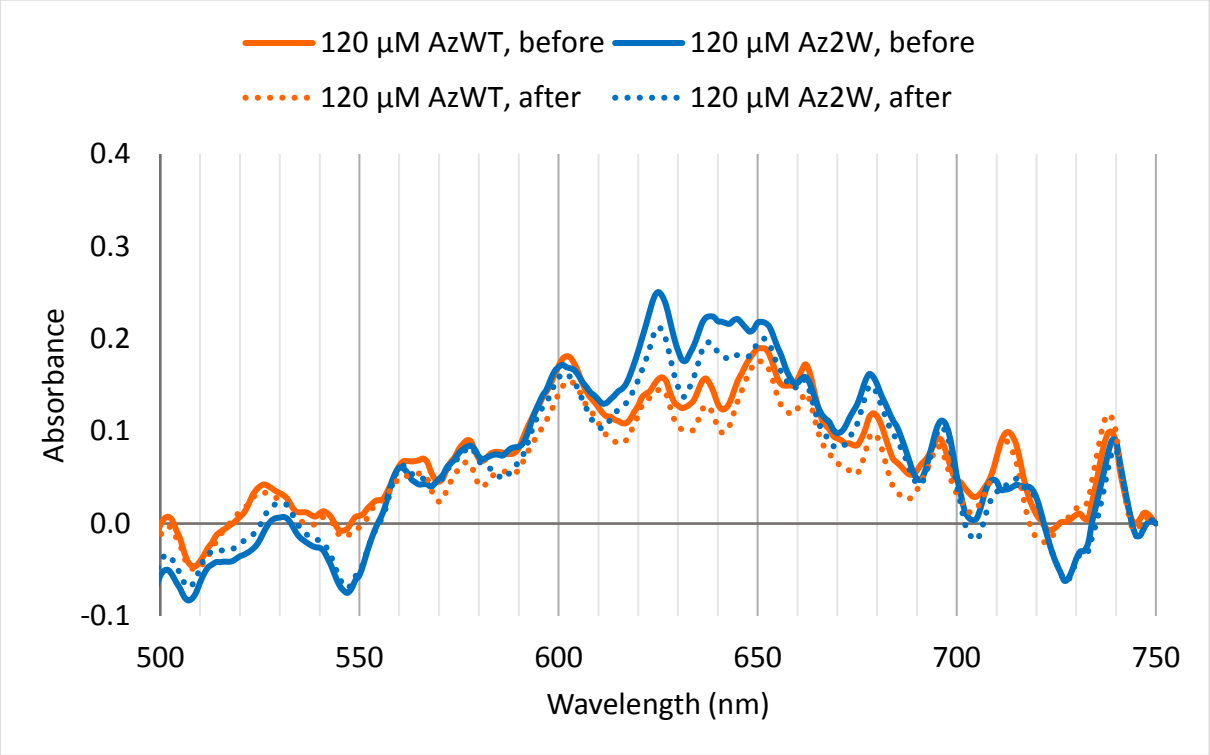

Figure 21 UV-VIS spectra of 120 µM samples of AzWT Met and Az2W Met. Same as on the previous figure, full lines – spectra before UV exposure, dotted lines – spectra after UV exposure. Enlarged area of the plot from 500 to 750 nm is shown. Only minor differences between spectra before and after can be observed in both proteins.

To summarize, when no photo-Met is present in the structure the A_{630} value (and thus protein redox state) is only minimally affected by photoactivation. On the other hand, in photo-Met-containing azurins a much more significant decrease was once again observed.

6. Discussion

Azurin expression and purification in nutritionally rich and limited media. We have successfully expressed wild type azurin and Az2W mutant with both Met and photo-Met (10–50% incorporation range) in the structure in LB and in-house prepared MM-M9 as well as commercially available DMEM-LM, respectively. Expression in DMEM-LM has yielded more total protein but photo-Met incorporation ratio was poor (in order of magnitude) compared to MM-M9. A possible explanation for this arises from lack of amino acids except for L-Gln in DMEM-LM formula since it has been previously reported that presence of inhibiting amino acids suppresses secondary pathways of amino acid synthesis [76].

The purification protocol we have previously published allowed us to successfully purify all of the expressed proteins. Azurin purification was already optimised as part of author's bachelor's thesis [43] and only minor alterations which allowed to slightly simplify and expedite the procedure were introduced.

Azurin oligomerization in solution detected by PIXL. As a result of PIXL experiments formation of cross-linked azurin dimers was observed in both AzWT and Az2W. MALDI-TOF MS analysis after trypsin and Lys-C in-gel digest has allowed us to confirm that SDS-PAGE protein bands (with 28−30 kDa relative mobility) we have attributed to azurin dimers exclusively provide azurin *m/z* signals, thus confirming their identity as azurin moieties. The intensity of the dimer bands on SDS-PAGE has shown to increase with total azurin concentration in the sample and was generally higher in Az2W mutant compared to equivalent AzWT samples, mainly in samples of lower protein concentration. We have also found that Az2W forms dimers even under the lowest studied 15 μM total azurin concentration while in wild type azurin dimer bands are not observed until 50 μM protein concentration is reached.

To map the cross-links, we have attempted to employ ESI-qTOF LC-MS/MS approach after trypsin proteolysis of dimer SDS-PAGE bands but the outcome of this experiment was not successful, since we were not able to detect an *m/z* signal corresponding to the linked peptides. Based on published azurin crystal structures (4AZU and 6MJS [44,77]) and our chemical XL data (see below) the interaction surface between azurin molecules in oligomers is formed by C-terminal β-sheets of two monomers which are most likely linked by adjacent photo-Met in position 109 (where Met residue is natively present) in PIXL experiment. When azurin is cleaved into peptides with trypsin this potential cross-linked product (linked pair of C-terminal peptides) has very high total mass which lays in the range where sensitivity of TOF analysers drops exponentially even for multiply charged ions which probably explains why we were not able to distinguish this *m/z* signal form noise in MS spectrum. To successfully determine the structure of the cross-link additional optimisation of protein digest procedure (e.g. use of a

different protease) and/or use of an MS analyser with higher resolution should be considered in the future.

PIXL vs. chemical XL. We have also employed chemical XL of the studied azurins with DSS and DSG to allow comparison with PIXL results. In this experiment formation of dimer (di) and intramolecularly linked azurin (i) were observed in AzWT (see Figure 22). Surprisingly, unlike with the wild type azurin, expected cross-linked dimer band (approx. 30 kDa relative mobility) was not present in Az2W samples.

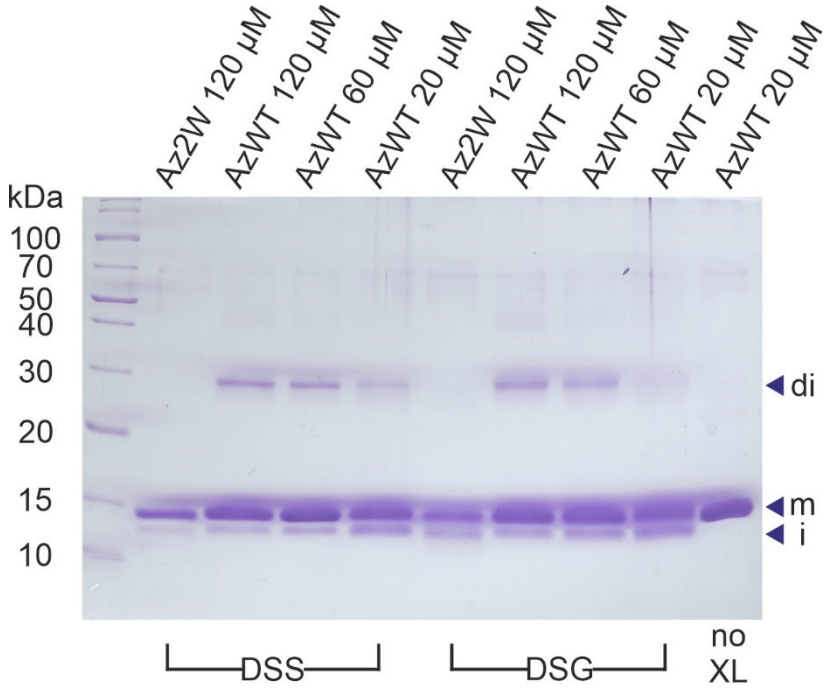

Figure 22 15% polyacrylamide electrophoretic gel with protein bands visualised with CBB-R250 showing the results of chemical XL experiment employing amine reactive DSS (11,4 Å spacer) and DSG (7,7 Å spacer) with AzWT and Az2W mutant at different concentrations (see labels at the top). All samples were diluted to 20 µM total azurin concentration before being loaded on gel. Type of used XL agent is listed at the bottom. The position of letters to the right corresponds with relative mobility of monomeric azurin (m), internally linked azurin (i) and azurin dimer (di). Internal cross-link is observed in all samples (except for control with no cross-linker) but surprisingly protein band corresponding to dimer is only present in AzWT samples. The intensity of dimer bands is generally lower when DSG is used to cross-link the protein. Results kindly provided by doc. RNDr. Miroslav Šulc, Ph.D.

This observation may lead to two conclusions. One can assume, that Az2W mutant does not form dimers, but such finding would be in contradiction with the literature [32,77] and our PIXL results. The other explanation for this discrepancy arises from the nature of cross-linking reagents used in the experiment. Since the reactive group in both DSS and DSG is an amine reactive NHS ester, the absence of dimer band in Az2W may imply that an amine group (most likely ε-amine of K) is no longer present on the interaction surface in this mutant. Incidentally, Az2W carries K122W modification which removes a K residue from C-terminal β-sheet, a structure known to play a role in azurin oligomerization [41].

Another argument to support this explanation and confirm the role K122 plays in XL formation arises from the intensity of the observed dimer bands in AzWT. In 4AZU crystal structure,

where azurin is present in the form of a tetramer, amine groups of K122 residues of two different azurin monomeric units lay on the interaction surface approx. 8–9 Å away from each other [44]. A shorter cross-linker like DSG (7,7 Å spacer arm) will have to be fully stretched and under a lot of steric tension to allow cross-link formation in such system, thus decreasing the yield of the reaction. On the other hand, DSS with 11,4 Å spacer will not encounter such limitation and the yield of linked dimer will not be affected. This exact observation arises from our results, noticeable mainly in the lowest tested azurin concentration (see Figure 22, p. 55, 20 μM samples)

Overall, this comparison of PIXL with DSS/DSG chemical XL shows one of the advantages of PIXL mentioned in the introduction (chapter 1.5 p. 23). Where chemical cross-linking reagents are dependent on the presence of a pair of appropriate target groups within a certain distance on the interaction surface of linked molecules, PIXL does not encounter such severe limitation since activated carben radical, which arises from photo-Met after UV activation, can react with any C–H or N–H bond in its immediate vicinity. Thus, the only requirement for successful photo-induced cross-linking being the presence of one Met (or Leu) residue on the interaction surface.

Photo induced electron release from activated photo-Met intermediate. In agreement with our earlier study we have once again observed ET reaction leading to reduction of Cu atom in azurin active site (detected through decrease of absorbance at 630 nm) in azurin samples after the protein was exposed to intense UV light.

In both studied proteins (AzWT and Az2W mutant) only minimal decrease of A_{630} occurred when no photo-Met was present in the protein sequence. The decrease that was observed in those control samples can be attributed to ET reaction initiated by intermediate reactive species formed from tryptophan residues during UV irradiation (an effect which was previously reported in azurin [78,79]). This hypothesis has been further discussed elsewhere [43], the most important point being that absence of any A_{630} value decrease in previously performed experiment with control All-Phe azurin mutant with no W in the sequence serves as an experimental proof of this claim.

Albeit not the only contributor, photo-Met plays the largest role in intriguing changes to azurin redox state observed during PIXL experiments. Photo-Met-containing azurins show several times higher relative decrease of A_{630} value when compared to Met controls. Which allows us to assume that UV activation of a photo-Met residue present in the structure leads to the introduction of a highly reactive intermediate which can serve as a potential electron donor for Cu atom in azurin active site. This process was observed in both wild type azurin and Az2W mutant with photo-Met. Interestingly, relative A_{630} decrease in both proteins increases with total azurin concentration in the sample. An intriguing reversal of this trend was observed in 15 μM Az2W. Under the lowest studied protein concentration relative decrease of A_{630} in this sample

has more than doubled to approx. 30% compared to 50 μM samples (not published data). Due to time constraints reproducibility of experiments with samples of low total azurin concentration was not yet tested and thus their results will not be used to draw any conclusions in this text, but the described discrepancy is worth further study.

It also warrants investigating which of the Met residues in azurin structure (when replaced with photo-Met) is responsible for the ET reaction. The axial ligand of Cu in the active site – M121 – is located directly in the primary coordination sphere of central metal atom (3,2 Å away from Cu [44]) and its replacement with photo-Met gives the highest chance of electron transferring directly from the activated intermediate to Cu atom. No other Met is present in 5 Å radius of azurin active site but contribution of two other Met residues in positions 13 and 44 (located 6,4 and 5,7 Å from Cu, respectively [44]) is also possible. Other Met residues are located further away from the active site and would require an electron hopping pathway to facilitate transfer of released electron to the active site. This mechanism can be estimated for M44 which is located beside G45 (as its carbonyl group is an axial ligand of Cu(II)). Moreover, electron hopping pathway seems particularly likely to occur in Az2W mutant where M109 is located within close proximity (approx. 5 Å) of C-terminal β-sheet and both W122 and W124 which were reported to participate in an ET process induced by a Re^{I}-complex anchored to H126 [77].

In the future site directed mutagenesis should be employed to determine the residue responsible for the process by removing individual Met residues (and thus photo-Met) from the sequence. Starting with the most likely "culprit", M121L mutants of both AzWT and Az2W should be constructed and if significant A_{630} decrease after photoactivation is no longer observed even in photo-Met azurins of this type, the role of this specific residue in ET process occurring during UV activation would be confirmed. Another speculative outcome of such experiment might be absence of A_{630} decrease in wild type azurin but only partial effect on Az2W construct due to the second ET process caused by electron hopping from M109 position occurring in this protein. M121L form of Az2W can then be used to design M121L H126M double mutant which would mirror the setup employed in the experiments with Re^{I}-labelled azurin [32,42] and allow us to compare PIER results in Az2W with an established ET initiation technique.

7. Conclusions

- We have successfully expressed wild type azurin (AzWT) and H83Q K122W T124W T126H All-Phe (Az2W) construct with Met in LB and purified the proteins based on previously optimised protocols.
- AzWT and Az2W with photo-Met in the structure were also successfully expressed in limited mediums and then purified.
  - Photo-Met incorporation ratio in commercial DMEM-LM was significantly lower than in in-house prepared MM-M9.
  - AzWT with 35−50% relative photo-Met incorporation and Az2W with 10−20% incorporation were produced.
- In PIXL experiments formation of cross-linked azurin dimers (based on MW) in both AzWT and Az2W was observed on SDS-PAGE.
  - The protein moiety of cross-linked product was confirmed as azurin by MALDI-TOF MS.
  - Az2W dimers were detected even in samples with 15 μM total azurin concentration. The intensity of dimer bands was overall higher in Az2W compared to AzWT, where dimers were only observed from 50 μM concentration.
  - While chemical XL with DSS/DSG encountered a complication due to the lack of K122 in Az2W construct, PIXL was capable of successfully cross-linking both proteins.
- The intriguing capability of photo-Met to release an electron and initiate ET process in azurin after photo-activation was once again observed – PIER is a promising potential technique.
  - Significantly higher A_{630} decrease (corresponding to central Cu atom reduction) after UV irradiation was observed in photo-Met-containing azurins when compared to Met proteins.
  - Site directed mutagenesis should be employed in the future to design azurin derivatives which would allow us to achieve a better understanding of this process, characterize the occurring reaction and compare PIER to an established ET initiation technique.

References

1. Gray, H. B. & Winkler, J. R. Electron transfer in proteins. *Annu. Rev. Biochem.* **65**, 537–561 (1996).
2. Fereiro, J. A. *et al.* Tunneling explains efficient electron transport via protein junctions. *Proc. Natl. Acad. Sci. U. S. A.* **115**, E4577–E4583 (2018).
3. Winkler, J. R. & Gray, H. B. Long-Range Electron Tunneling. *J. Am. Chem. Soc.* **136**, 2930–2939 (2014).
4. Warren, J. J., Ener, M. E., Vlček Jr., A., Winkler, J. R. & Gray, H. B. Electron hopping through proteins. *Coord. Chem. Rev.* **256**, 2478–2487 (2012).
5. Gray, H. B. & Winkler, J. R. Long-range electron transfer. *Proc. Natl. Acad. Sci. U. S. A.* **102**, 3534–3539 (2005).
6. Hagras, M. A. & Stuchebrukhov, A. A. Electron tunneling in proteins program. *J. Comput. Chem.* **37**, 1388–1395 (2016).
7. Blanco-Rodriguez, A. M. *et al.* Phototriggering Electron Flow through Re-I-modified Pseudomonas aeruginosa Azurins. *Chem.- Eur. J.* **17**, 5350–5361 (2011).
8. Möbius, K., Savitsky, A., Schnegg, A., Plato, M. & Fuchs, M. High-field EPR spectroscopy applied to biological systems: characterization of molecular switches for electron and ion transfer. *Phys. Chem. Chem. Phys.* **7**, 19–42 (2005).
9. Hosseinzadeh, P. & Lu, Y. Design and Fine-tuning Redox Potentials of Metalloproteins Involved in Electron Transfer in Bioenergetics. *Biochim. Biophys. Acta* **1857**, 557–581 (2016).
10. de la Lande, A., Gillet, N., Chen, S. & Salahub, D. R. Progress and challenges in simulating and understanding electron transfer in proteins. *Arch. Biochem. Biophys.* **582**, 28–41 (2015).

11. Gutierrez, A., Lian, L.-Y., Wolf, C. R., Scrutton, N. S. & Roberts, G. C. K. Stopped-flow kinetic studies of flavin reduction in human cytochrome P450 reductase and its component domains. *Biochemistry* **40**, 1964–1975 (2001).
12. Haffa, A. L. M. *et al.* The dependence of the initial electron-transfer rate on driving force in Rhodobacter sphaeroides reaction centers. *J. Phys. Chem. B* **106**, 7376–7384 (2002).
13. Crane, B. R., Di Bilio, A. J., Winkler, J. R. & Gray, H. B. Electron tunneling in single crystals of Pseudomonas aeruginosa azurins. *J. Am. Chem. Soc.* **123**, 11623–11631 (2001).
14. Hammi, E. E. *et al.* New insights into the mechanism of electron transfer within flavohemoglobins: Tunnelling pathways, packing density, thermodynamic and kinetic analyses. *Phys. Chem. Chem. Phys.* **14**, 13872–13880 (2012).
15. Millett, F., Havens, J., Rajagukguk, S. & Durham, B. Design and use of photoactive ruthenium complexes to study electron transfer within cytochrome bc1 and from cytochrome bc1 to cytochrome c. *Biochim. Biophys. Acta - Bioenerg.* **1827**, 1309–1319 (2013).
16. Heyes, D. J. *et al.* Internal electron transfer in multi-site redox enzymes is accessed by laser excitation of thiouredopyrene-3,6,8-trisulfonate (TUPS). *Chem. Commun.* 1124–1126 (2009) doi:10.1039/b820386e.
17. Bhattacharyya, A. K., Lipka, J. J., Waskell, L. & Tollin, G. Laser Flash Photolysis Studies of the Reduction Kinetics of NADPH:Cytochrome P-450 Reductase. *Biochemistry* **30**, 759–765 (1991).
18. Nersissian, A. M. & Shipp, E. L. Blue copper-binding domains. *Adv. Protein Chem.* **60**, 271–340 (2002).
19. Messerschmidt, A. *et al.* Refined crystal structure of ascorbate oxidase at 1.9 Å resolution. *J. Mol. Biol.* **224**, 179–205 (1992).

20. Faraggi, M. & Pecht, I. The reaction of Pseudomonas azurin with hydrated electrons. *Biochem. Biophys. Res. Commun.* **45**, 842–848 (1971).

21. Wherland, S., Holwerda, R. A., Rosenberg, R. C. & Gray, H. B. Kinetic studies of the reduction of blue copper proteins by iron(EDTA)2-. *J. Am. Chem. Soc.* **97**, 5260–5262 (1975).

22. Margalit, R. *et al.* Preparation and characterization of pentaammineruthenium-(histidine-83)azurin: thermodynamics of intramolecular electron transfer from ruthenium to copper. *Proc. Natl. Acad. Sci.* **81**, 6554–6558 (1984).

23. Yanagisawa, S. & Dennison, C. Loop-Contraction Mutagenesis of a Type 1 Copper Site. *J. Am. Chem. Soc.* **125**, 4974–4975 (2003).

24. Hosseinzadeh, P. *et al.* Design of a single protein that spans the entire 2-V range of physiological redox potentials. *Proc. Natl. Acad. Sci.* **113**, 262–267 (2016).

25. Marshall, N. M. *et al.* Rationally tuning the reduction potential of a single cupredoxin beyond the natural range. *Nature* **462**, 113–116 (2009).

26. Romero, A. *et al.* X-ray Analysis and Spectroscopic Characterization of M121Q Azurin. *J. Mol. Biol.* **229**, 1007–1021 (1993).

27. Alcaraz, L. A. & Donaire, A. Rapid binding of copper(I) to folded aporusticyanin. *FEBS Lett.* **579**, 5223–5226 (2005).

28. Engeseth, H. R. & McMillin, D. R. Studies of thermally induced denaturation of azurin and azurin derivatives by differential scanning calorimetry: evidence for copper selectivity. *Biochemistry* **25**, 2448–2455 (1986).

29. Pérez-Henarejos, S. A., Alcaraz, L. A. & Donaire, A. Blue Copper Proteins: A rigid machine for efficient electron transfer, a flexible device for metal uptake. *Arch. Biochem. Biophys.* **584**, 134–148 (2015).

30. Adman, E. T. Copper Protein Structures. in *Advances in Protein Chemistry* (ed. C.B. Anfinsen, J. T. E., Frederic M. Richards and David S. Eisenberg) vol. 42 145–197 (Academic Press, 1991).
31. Nar, H., Messerschmidt, A., Huber, R., van de Kamp, M. & Canters, G. W. Crystal structure of Pseudomonas aeruginosa apo-azurin at 1.85 Å resolution. *FEBS Lett.* **306**, 119–124 (1992).
32. Takematsu, K. *et al.* Hole Hopping Across a Protein–Protein Interface. *J. Phys. Chem. B* **123**, 1578–1591 (2019).
33. Dennison, C. Investigating the structure and function of cupredoxins. *Coord. Chem. Rev.* **249**, 3025–3054 (2005).
34. Rosen, P. & Pecht, I. Conformational equilibria accompanying the electron transfer between cytochrome c (P551) and azurin from Pseudomonas aeruginosa. *Biochemistry* **15**, 775–786 (1976).
35. van de Kamp, M., Hali, F. C., Rosato, N., Agro, A. F. & Canters, G. W. Purification and characterization of a non-reconstitutable azurin, obtained by heterologous expression of the Pseudomonas aeruginosa azu gene in Escherichia coli. *Biochim. Biophys. Acta* **1019**, 283–292 (1990).
36. Nar, H. *et al.* Characterization and crystal structure of zinc azurin, a by-product of heterologous expression in Escherichia coli of Pseudomonas aeruginosa copper azurin. *Eur. J. Biochem.* **205**, 1123–1129 (1992).
37. McLaughlin, M. P. *et al.* Azurin as a protein scaffold for a low-coordinate nonheme iron site with a small-molecule binding pocket. *J. Am. Chem. Soc.* **134**, 19746–19757 (2012).
38. Bonander, N. *et al.* The metal site of Pseudomonas aeruginosa azurin, revealed by a crystal structure determination of the co(II) derivative and co-EPR spectroscopy. *Proteins Struct. Funct. Bioinforma.* **27**, 385–394 (1997).

39. Pascher, T., Karlsson, B. G., Nordling, M., Malmström, B. G. & Vänngård, T. Reduction potentials and their pH dependence in site-directed-mutant forms of azurin from Pseudomonas aeruginosa. *Eur. J. Biochem.* **212**, 289–296 (1993).

40. Garner, D. K. *et al.* Reduction Potential Tuning of the Blue Copper Center in Pseudomonas aeruginosa Azurin by the Axial Methionine as Probed by Unnatural Amino Acids. *J. Am. Chem. Soc.* **128**, 15608–15617 (2006).

41. Sokolová, L. *et al.* Mass spectrometric characterization of oligomers in Pseudomonas aeruginosa azurin solutions. *J. Phys. Chem. B* **115**, 4790–4800 (2011).

42. Takematsu, K. *et al.* Tryptophan-Accelerated Electron Flow Across a Protein–Protein Interface. *J. Am. Chem. Soc.* **135**, 15515–15525 (2013).

43. Tuzhilkin, R. Studium strukturně funkčních vztahů elektrotransportních proteinových systémů. (2018).

44. Nar, H., Messerschmidt, A., Huber, R., van de Kamp, M. & Canters, G. W. Crystal structure analysis of oxidized Pseudomonas aeruginosa azurin at pH 5·5 and pH 9·0. *J. Mol. Biol.* **221**, 765–772 (1991).

45. Murata, K. & Wolf, M. Cryo-electron microscopy for structural analysis of dynamic biological macromolecules. *Biochim. Biophys. Acta Gen. Subj.* **1862**, 324–334 (2018).

46. Mitra, A. K. Visualization of biological macromolecules at near-atomic resolution: cryo-electron microscopy comes of age. *Acta Crystallogr. Sect. F Struct. Biol. Commun.* **75**, 3–11 (2019).

47. Young, M. M. *et al.* High throughput protein fold identification by using experimental constraints derived from intramolecular cross-links and mass spectrometry. *Proc. Natl. Acad. Sci. U. S. A.* **97**, 5802–5806 (2000).

48. Back, J. W., de Jong, L., Muijsers, A. O. & de Koster, C. G. Chemical cross-linking and mass spectrometry for protein structural modeling. *J. Mol. Biol.* **331**, 303–313 (2003).

49. Sinz, A. Chemical cross-linking and mass spectrometry for mapping three-dimensional structures of proteins and protein complexes. *J. Mass Spectrom. JMS* **38**, 1225–1237 (2003).

50. Sinz, A. Chemical cross-linking and mass spectrometry to map three-dimensional protein structures and protein–protein interactions. *Mass Spectrom. Rev.* **25**, 663–682 (2006).

51. Leitner, A. *et al.* Probing Native Protein Structures by Chemical Cross-linking, Mass Spectrometry, and Bioinformatics. *Mol. Cell. Proteomics MCP* **9**, 1634–1649 (2010).

52. Lomant, A. J. & Fairbanks, G. Chemical probes of extended biological structures: Synthesis and properties of the cleavable protein cross-linking reagent [35S]dithiobis(succinimidyl propionate). *J. Mol. Biol.* **104**, 243–261 (1976).

53. Cuatrecasas, P. & Parikh, I. Adsorbents for affinity chromatography. Use of N-hydroxysuccinimide esters of agarose. *Biochemistry* **11**, 2291–2299 (1972).

54. Hartman, F. C. & Wold, F. Bifunctional Reagents. Cross-Linking of Pancreatic Ribonuclease with a Diimido Ester1. *J. Am. Chem. Soc.* **88**, 3890–3891 (1966).

55. Hoare, D. G. & Koshland, D. E. A Procedure for the Selective Modification of Carboxyl Groups in Proteins. *J. Am. Chem. Soc.* **88**, 2057–2058 (1966).

56. Staros, J. V., Wright, R. W. & Swingle, D. M. Enhancement by N-hydroxysulfosuccinimide of water-soluble carbodiimide-mediated coupling reactions. *Anal. Biochem.* **156**, 220–222 (1986).

57. Vasilescu, J., Guo, X. & Kast, J. Identification of protein-protein interactions using in vivo cross-linking and mass spectrometry. *PROTEOMICS* **4**, 3845–3854 (2004).

58. Prescher, J. A. & Bertozzi, C. R. Chemistry in living systems. *Nat. Chem. Biol.* **1**, 13–21 (2005).

59. Gilchrist, T. L. & Rees, C. W. Carbenes, nitrenes and arynes. (1969).

60. Suchanek, M., Radzikowska, A. & Thiele, C. Photo-leucine and photo-methionine allow identification of protein-protein interactions in living cells. *Nat. Methods* **2**, 261–267 (2005).

61. Kalkhof, S., Ihling, C., Mechtler, K. & Sinz, A. Chemical Cross-Linking and High-Performance Fourier Transform Ion Cyclotron Resonance Mass Spectrometry for Protein Interaction Analysis: Application to a Calmodulin/Target Peptide Complex. *Anal. Chem.* **77**, 495–503 (2005).

62. Šulc, M. & Ptáčková, R. Biotechnologické aspekty UV-světlem iniciovaného síťování – PIXL (z angl. Photo -Induced Cross -Linking): nové alternativní techniky pro studium 3D struktury proteinů či vzájemných interakcí. *Bioprospect Bull. Biotechnol. Spol. V Čes. Republice Slov. Republice* **26**, 79–83 (2016).

63. Silvian, L. F., Wang, J. & Steitz, T. A. Insights into Editing from an Ile-tRNA Synthetase Structure with tRNA^{Ile} and Mupirocin. *Science* **285**, 1074–1077 (1999).

64. Deniziak, M. A. & Barciszewski, J. Methionyl-tRNA synthetase. *Acta Biochim. Pol.* **48**, 337–350 (2001).

65. Dayhoff, M., Hunt, L. & Hurst-Calderone, S. Composition of proteins. *Atlas Protein Seq. Struct.* **5**, 363–373 (1978).

66. Koberova, M. *et al.* Photo-cytochrome b(5) - A New Tool to Study the Cytochrome P450 Electron-transport Chain. *Int. J. Electrochem. Sci.* **8**, 125–134 (2013).

67. Kiick, K. L. & Tirrell, D. A. Protein engineering by in vivo incorporation of non-natural amino acids: Control of incorporation of methionine analogues by methionyl-tRNA synthetase. *Tetrahedron* **56**, 9487–9493 (2000).

68. Ptackova, R. *et al.* The Application of an Emerging Technique for Protein-Protein Interaction Interface Mapping: The Combination of Photo-Initiated Cross-Linking Protein Nanoprobes with Mass Spectrometry. *Int. J. Mol. Sci.* **15**, 9224–9241 (2014).

69. Ječmen, T. *et al.* Photo-initiated crosslinking extends mapping of the protein-protein interface to membrane-embedded portions of cytochromes P450 2B4 and b5. *Methods* **89**, 128–137 (2015).

70. Gonçalves, M. R. & Frin, K. P. M. Synthesis, characterization, photophysical and electrochemical properties of rhenium(I) tricarbonyl diimine complexes with triphenylphosphine ligand. *Polyhedron* **132**, 20–27 (2017).

71. Blanco-Rodríguez, A. M. *et al.* Excited-State Dynamics of Structurally Characterized [ReI(CO)3(phen)(HisX)]+ (X = 83, 109) Pseudomonas aeruginosa Azurins in Aqueous Solution. *J. Am. Chem. Soc.* **128**, 4365–4370 (2006).

72. Vlček, A., Kvapilová, H., Towrie, M. & Záliš, S. Electron-Transfer Acceleration Investigated by Time Resolved Infrared Spectroscopy. *Acc. Chem. Res.* **48**, 868–876 (2015).

73. Marazzi, M., Gattuso, H., Fumanal, M., Daniel, C. & Monari, A. Charge-Transfer versus Charge-Separated Triplet Excited States of [ReI(dmp)(CO)3(His124)(Trp122)]+ in Water and in Modified Pseudomonas aeruginosa Azurin Protein. *Chem. – Eur. J.* **25**, 2519–2526 (2019).

74. Reece, S. Y., Lutterman, D. A., Seyedsayamdost, M. R., Stubbe, J. & Nocera, D. G. Re(bpy)(CO)3CN as a Probe of Conformational Flexibility in a Photochemical Ribonucleotide Reductase. *Biochemistry* **48**, 5832–5838 (2009).

75. Dunn, A. R. *et al.* Luminescent Ruthenium(II)− and Rhenium(I)−Diimine Wires Bind Nitric Oxide Synthase. *J. Am. Chem. Soc.* **127**, 5169–5173 (2005).

76. Zaslaver, A. *et al.* Just-in-time transcription program in metabolic pathways. *Nat. Genet.* **36**, 486–491 (2004).

77. Takematsu, K. *et al.* Two Tryptophans Are Better Than One in Accelerating Electron Flow through a Protein. *ACS Cent. Sci.* **5**, 192–200 (2019).

78. Westerlund, K., Berry, B. W., Privett, H. K. & Tommos, C. Exploring amino-acid radical chemistry: protein engineering and de novo design. *Biochim. Biophys. Acta BBA - Bioenerg.* **1707**, 103–116 (2005).

79. Larson, B. C. *et al.* Photogeneration and Quenching of Tryptophan Radical in Azurin. *J. Phys. Chem. B* **119**, 9438–9449 (2015).